We are IntechOpen, the world's leading publisher of Open Access books Built by scientists, for scientists

4,800
Open access books available

122,000
International authors and editors

135M
Downloads

Our authors are among the

154
Countries delivered to

TOP 1%
most cited scientists

12.2%
Contributors from top 500 universities

CLARIVATE ANALYTICS
BOOK CITATION INDEX
INDEXED

WEB OF SCIENCE™

Selection of our books indexed in the Book Citation Index
in Web of Science™ Core Collection (BKCI)

Interested in publishing with us?
Contact book.department@intechopen.com

Numbers displayed above are based on latest data collected.
For more information visit www.intechopen.com

Contemporary Forming Methods of the Structure and Properties of Cast Magnesium Alloys

Leszek Adam Dobrzański, Tomasz Tański, Szymon Malara,
Mariusz Król and Justyna Domagała-Dubiel
Division of Materials Processing Technology
Management and Computer Techniques in Materials Science
Institute of Engineering Materials and Biomaterials
Silesian University of Technology
ul. Konarskiego 18a, 44-100 Gliwice
Poland

1. Introduction

For the reason of growing requirements for materials made from light alloys concerning mechanical properties, corrosion resistance, manufacturing costs and the influence of the environment this efforts can be consider as very up-to-date from the scientistic view and very attractive for investigation.

The rising tendencies of magnesium alloy production, show increased need of their application in world industry and what follows the magnesium alloys become one of the most often apply construction material our century.

A contemporary technological development makes it necessary to look for new constructional solutions that aim at the improvement of the effectiveness and quality of a product, at the minimization of dimension and mass as well as the increasing of reliability and dimension stability in the operation conditions. For a dozen or so years one can observe a rising interest in the non-ferrous metals alloys including magnesium alloys which are an examination subject in many research and university centres in the country and abroad as well as in major manufacturers of mechanical engineering industry, chemical, power, textile, electronic, paper and aeronautic industries and in particular automotive, shipbuilding, aircraft, sports and even nuclear industries (Baker, 1999; Dobrzański and Tański, 2009; Fajkiel and Dudek, 2004).

Magnesium alloys which are successfully used for a long time in different industry branches are a combination of low density and high strength. The above features together with low inertia have significantly contributed to the wide use of magnesium alloys in fast moving elements, in locations where rapid velocity changes occur and in products in which lowering a final mass of a product is required. The greatest interest in magnesium alloys was shown and is still shown by an automotive industry (Figure 1) (Horst and Mordike, 2006; Kainem, 2003; Tański *et al.*, 2007). For example, *General Motors* in their big cars (Savana

& Express) use 26.3 kg of magnesium cast alloys, and in smaller cars (Safari, Astro) – 165 kg, Ford F – 150 – 14.5 kg, VW Passat and Audi A4 and A6 from 13.6 to 14.5 kg, Alfa Romeo – 9.3kg. A further demand for magnesium casts is expected, of up to 50 kg per each car. It is mainly because of the fact that the magnesium casts have got a low density (1700-1900 kg/m³), and at the same time, their mechanical properties are similar to the aluminium casting alloys.

| Cylinder head cover | Wheel bands | Car inside |

| Casing of the minidisk | Housing of the phone | Housing of the photographic camera |

Fig. 1. Elements from magnesium alloys

A desire to create as light vehicle constructions as possible and connected with it low fuel consumption have made it possible to make use of magnesium alloys as a constructional material in car wheels, engine pistons, gear box and clutch housings, skeletons of sunroofs, framing of doors, pedals, suction channels, manifolds, housings of propeller shafts, differential gears, brackets, radiators and others. Moreover, the magnesium alloys demonstrate good corrosion resistance, no aggressiveness towards the mould material and low heat of fusion what enables the use of pressure die casting ensuring good shape reproducibility (Kainem, 2003; Kiełbus et al., 2006; Maltaisa et al., 2004; Rzychoń and Kiełbus, 2007). Magnesium alloys have also found their application in manufacturing of mowers, saws, robots, office equipment including computer hardware, sport and medical appliances, in production of movie and video cameras, for rocket parts, space ships, and others (Dobrzański and Tański, 2009).

The increasing use of magnesium alloys is caused by the progress in the manufacturing of new reliable alloys with the addition of Zr, Ce i Cd and very light alloys are made from Li. A general tendency of a present stage of cast materials development is the increase of their plasticity together with the increase of their resistance properties (Figure 2) (Fajkiel and Dudek, 2004).

In order to effectively control microstructure development during the melting, solidification as well as further materials processing is necessary to understand all metallurgical

phenomena taking place. Knowledge of the solidification process as well as the influence of liquid and/or semi solid metal treatment on micro and macro structure characteristic is of primary importance. The simples and very effective method, which make it possible to determine a curve of the crystallization process – the cool curve $T=F(t)$, is thermal analysis. Advanced Thermal Analysis (TA) techniques monitor the temperature changes in sample as it cools through a phase transformation interval (Backuerud et al., 1990; Emandi et al., 2005; MacKay et al., 2000). The temperature changes in the materials are recorded as a function of the heating or cooling time in such a manner that allows for the detection phase transformation. In order to increase accuracy, characteristic points on the cooling curve have been identified using the first derivative curve plotted versus time (Kasprzak et al., 2008; Kierkus & Sokolowski, 1999; Patent No.: US 7,354,491 B2).
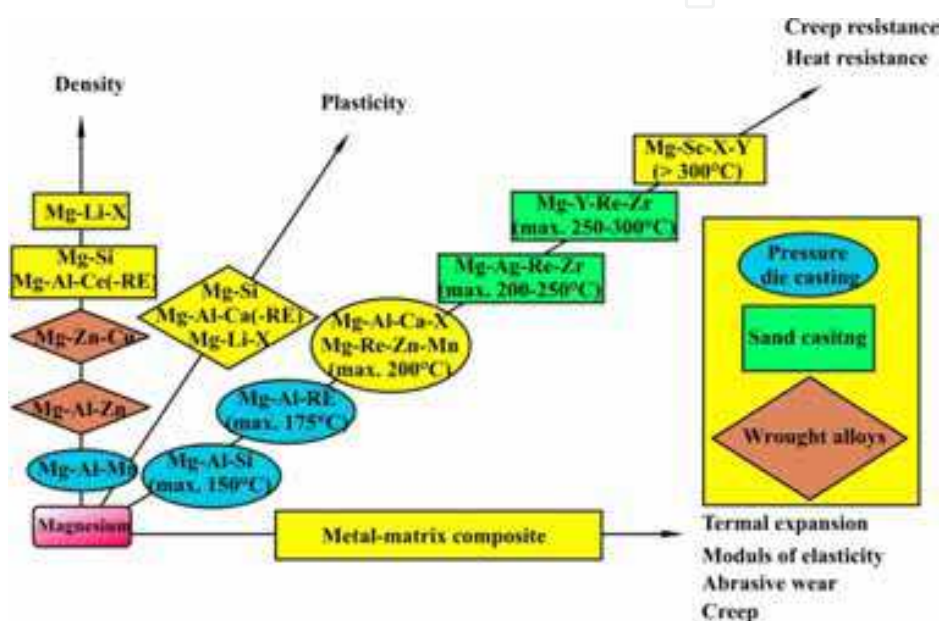

Fig. 2. Potential development directions of New magnesium alloys (Fajkiel and Dudek, 2004)

Increasing of surface layers properties can by achieved by many technologies i.e.: electroplating, anodizing, PVD, laser alloying or padding. Main advantages of laser treatment are i.e.: short time of process, flexibility or operation precision (Bachmann, 2003; Vollertsen and Partes, 2005).

Main goal of surface laser treatment is modification structure and properties. Increasing of wear resistance is creation of result of chemical homogeneous, fine-crystalline of surface layer without chemical changes. More advantageous properties can be achieved by alloying with hard particles of carbides, oxides or nitrides (Barnes et al., 2003; Cao et al., 2008; Dobrzański et al., 2008; Dutta Majumdar et al., 2003; Yadroitsev et al., 2007).

Laser technologies are the most of promise and effective for assurance of continuous development of materials processing branch as a results of forecasts concerning global economic development. One considers that economies, which make use of laser technologies on a large scale, will be competitive on the global market (Bachmann, 2003; Vollertsen and Partes, 2005).

The rising tendencies of magnesium alloy production, show increased need of their application in world industry and what follows the magnesium alloys become one of the most often apply construction material our century. Therefore it is extremely important to

keep a high investigation development of a light alloy issue, furthermore performing in Institute of Material Processes and Computer Technology, Institute of Engineering Materials and Biomaterials, Silesian University of Technology.

The goal of this paper is to present of the investigation results of the casting magnesium alloy in its as-cast state and after heat and surface laser treatment.

2. Experimental procedure

2.1 Materials

The investigations have been carried out on test pieces of MCMgAl12Zn1 (Table 1, No. 1), MCMgAl9Zn (Table 1, No.2), MCMgAl6Zn (Table 1, No. 3), MCMgAl3Zn (Table 1, No. 4) magnesium alloys in as-cast and after heat treatment states. The chemical composition of the investigated materials is given in Table 1. A casting cycle of alloys has been carried out in an induction crucible furnace using a protective salt bath *Flux 12* equipped with two ceramic filters at the melting temperature of 750±10ºC, suitable for the manufactured material. In order to maintain a metallurgical purity of the melting metal, a refining with a neutral gas with the industrial name of *Emgesalem Flux 12* has been carried out. To improve the quality of a metal surface a protective layer *Alkon M62* has been applied. The material has been cast in dies with betonite binder because of its excellent sorption properties and shaped into plates of 250x150x25 mm. The cast alloys have been heated in an electrical vacuum furnace *Classic 0816 Vak* in a protective argon atmosphere.

No.	Al	Zn	Mn	Si	Fe	Mg	Rest
1	12.1	0.62	0.17	0.047	0.013	86.96	0.0985
2	9.09	0.77	0.21	0.037	0.011	89.79	0.0915
3	5.92	0.49	0.15	0.037	0.007	93.33	0.0613
4	2.96	0.23	0.09	0.029	0.006	96.65	0.0361

The mass concentration of main elements, %

Table 1. Chemical composition of investigated alloys, %

2.2 Heat treatment

The applied heat treatment was performed according to the determined scheme (Table 2)

Sing the state of heat treatment	Solution treatment			Aging treatment		
	Temperature	Time	Cooling	Temperature	Time	Cooling
0	**As-cast**					
1	430	10	air	-	-	-
2	430	10	water	-	-	-
3	430	10	furnace	-	-	-
4	430	10	water	190	15	air

Table 2. Parameters of heat treatment of investigated alloys

2.3 Thermal analysis

The thermo-derivative analysis was performed with the Mg-Al-Zn alloys using the UMSA (Universal Metallurgical Simulator and Analyzer) device (Patent No.: US 7,354,491 B2). The carrying out of the thermo analysis using the UMSA device was based on remelting, heating and cooling of the sample with a proper established cooling rate. The samples with a shape and size showed on Fig. 3 were induction heated to the temperature at 700±1°C.
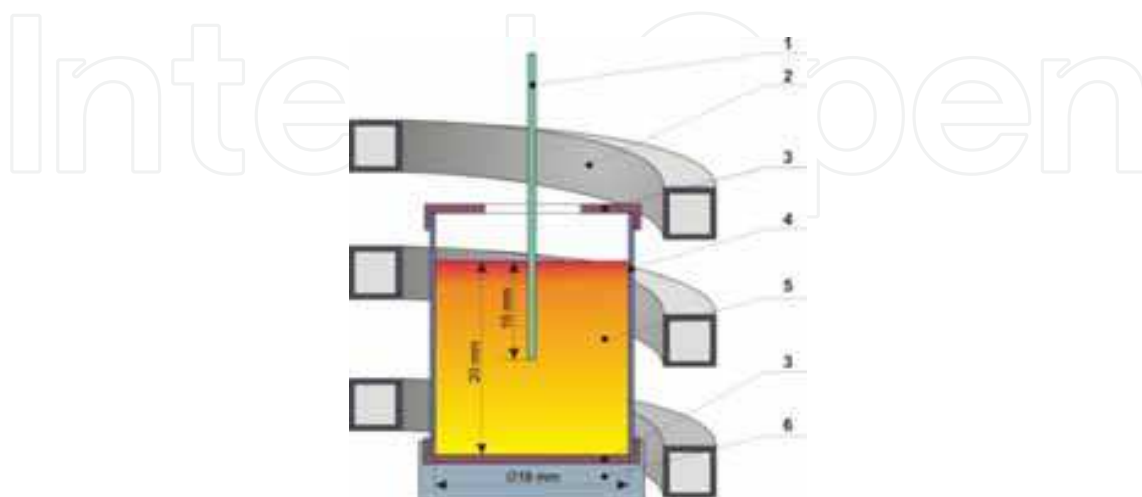

Fig. 3. Scheme of the UMSA Thermal Analysis Platform experimental set-up: 1 – low thermal mass thermocouple, 2 – heating and cooling coil, 3 – thermal insulation, 4 – steel foil, 5 – test sample, 6 – ceramic base.

For achieving of the cooling rate of:
-   ≈ 0,6°C/s the sample was freely cooled,
-   ≈ 1,2°C/s by a cooling system with argon using a flow rate 30 l/min,
-   ≈ 2,4°C/s by a cooling system with argon using a flow rate 125 l/min.

On the basis of the ATD analysis there were determined the characteristic points describing the thermal phenomena present during the alloy crystallisation, which define the temperature and time values of the thermo-derivative analyse curves.

2.4 Laser treatment

The analysis of the surface modification influence using the high power diode laser HPDL Rofin DL 020 was performed for Mg-Al-Zn cast magnesium alloys alloyed with titanium, tungsten, vanadium, niobium and silicon carbides, as well with aluminium oxide (Table 3).

Properties	WC	TiC	VC	NbC	SiC	TaC	Al_2O_3
Density, kg/m³	15.69	4.25	5.36	7.60	3.44	15.03	3.97
Hardness, HV	3400	1550	2850	2100	1600	1725	2300
Melting temperature, ᵒC	2870	3140	2830	3500	1900	3880	2047
Mean grain size, µm	0.7-0.9	< 1.0		<10	<10	<10	1-5
	>5	>6.4	>1.8	<45	<75	<45	80

Table 3. Properies of ceramic powders used to laser alloying

The laser treatment of the cast magnesium alloys was performed using the permanent powder feed technique into the alloying zone area by a granulate dosage using a fluidisation feeder. The powder feeder was connected to the feeding gas cylinder as well to the powder-feeding nozzle. In the powder feeding system the feed rate of the carrier gas was set by 5 l/min. After preliminary tests the laser power for investigations was set in a range of 1.2-2.0 kW and a laser alloying rate of 0.25; 0.50; 0.75; 1.00 m/min was chosen.

The investigations has revealed that the optimal geometry of a single laser tray was achieved by an alloying rate of 0.75 m/min except the Al_2O_3 and NbC powders, where the optimal alloying rate was set like 0.50 m/min and 0.25 m/min respectively.

2.5 Specimens characterization

The observations of the investigated cast materials have been made on the light microscope LEICA MEF4A as well as on the electron scanning microscope ZEISS SUPRA 25. The X-ray qualitative and quantitative microanalysis and the analysis of a surface distribution of cast elements in the examined magnesium cast alloy specimens in as-cast and after heat, laser treatment have been made on transverse microsections on the ZEISS SUPRA 25 scanning microscope with the. Phase composition and crystallographic structure were determined by the X-ray diffraction method using the X`Pert device with a cobalt lamp, with 40 kV voltage. The measurement was performed in angle range of 2 Θ: 20° - 120°. Hardness tests were made using Zwick ZHR 4150 TK hardness tester in the HRF scale. Compression and tensile tests were made using Zwick Z100 testing machine. Microhardness of the cross section of the laser surface melted layer was measured on Fully-Automatic Microhardness Testing System with a loading time of 15 s and the testing load of 100 g.

3. Results and discussions

3.1 Heat treatment

The results of metallographic investigations performed on light and scanning electron microscope (Figs. 4-6), confirmed also by appliance of the EDS surface analysis, quantitative EDS point wise microanalysis and X-Ray diffraction (Figs. 7-8, Table 4) it has been confirmed that the magnesium cast alloys MCMgAl12Zn1, MCMgAl9Zn1, MCMgAl6Zn1, MCMgAl3Zn1 in the cast state are characterized by a microstructure of the solid solution α constituting the alloy matrix as well as the γ – $Mg_{17}Al_{12}$ discontinuous intermetallic phase in the forms of plates located mostly at grain boundaries. Moreover, in the vicinity of the γ intermetallic phase precipitations the presence of the needle eutectics (α + γ) has been revealed.

In the structure of the examined magnesium cast alloys one can observe, apart from $Mg_{17}Al_{12}$ precipitations, turning grey phases, characterized by angular contour with smooth edges in the shape of hexahedrons (Fig. 4). Out of the chemical composition examinations with the use of the EDS dispersive radiation spectrometer (Fig. 8, Table 4) as well as literature data, one can conclude that it is the Mg_2Si compound which, when precipitating, increases the hardness of castings . There have appeared, after the process of solutioning with cooling in water and in the air, trace quantities of the γ ($Mg_{17}Al_{12}$) phase and single precipitations of a light grey phase and Mn-Al-Fe precipitation in the structure of the alloy. There have not been noticed any locations of eutectic occurrences in the structure (Fig. 5a).

However for the MCMgAl12Zn1 alloy there was found numerous areas of the γ phase – which was not dissolved in the matrix, as well some eutectics (Fig. 5b).

After the cooling bell annealing the structure of the solid solution α with many precipitations of the secondary phase γ has been revealed (locations resembling eutectics). The precipitations of the γ ($Mg_{17}Al_{12}$) phase, located at grain boundaries and the light grey phase located mostly at the phase β boundary have also been observed. The structure of this alloy is similar to the structure of the as-cast alloy (Fig. 6a). The applied ageing process after the solution heat treatment with cooling in the air has caused the release of the γ phase at grain boundaries as well as in the form of pseudo eutectic locations. There have been revealed, in the structure of the material, the parallel twinned crystals extending along the whole grain (Fig. 6b).
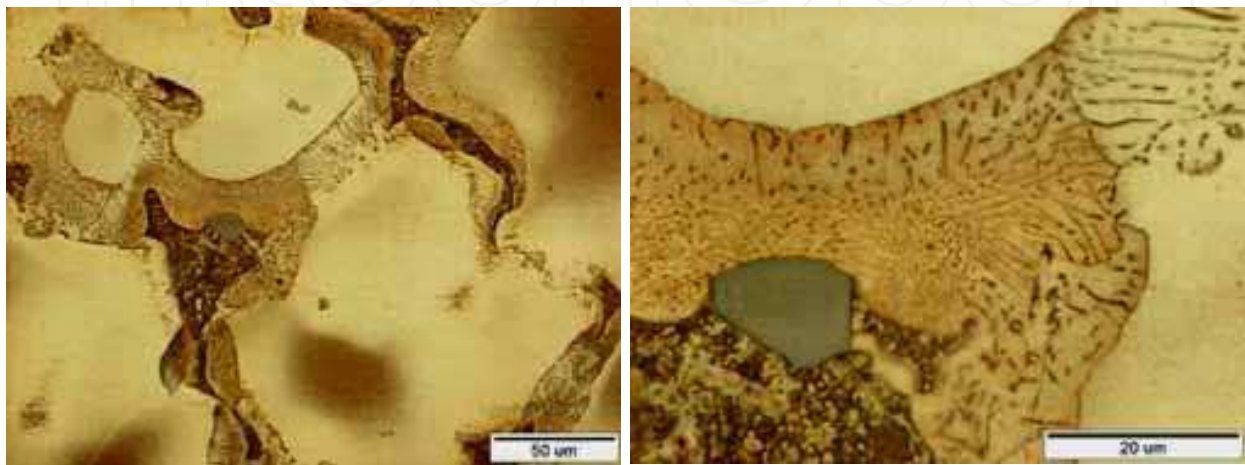
Fig. 4. Structure of the MCMgAl9Zn1 magnesium cast alloy in as- cast state

(a)   (b)
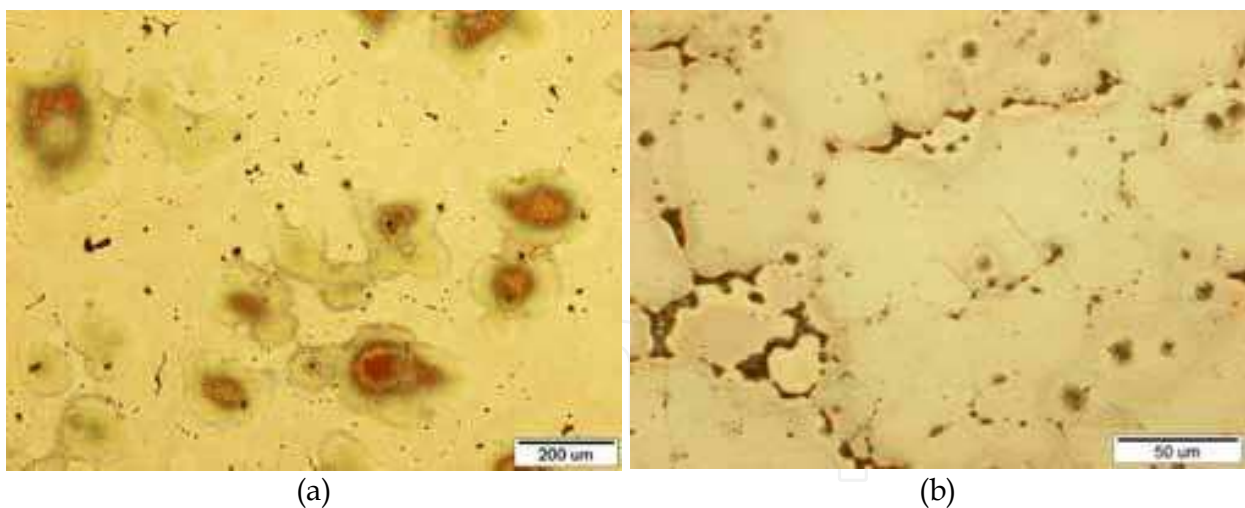
Fig. 5. Structure of the magnesium cast alloy: a) MCMgAl3Zn1 after solutioning with cooling in the air; b) MCMgAl12Zn1 after solutioning with cooling in water

The chemical analysis of the surface element decomposition and the quantitative micro analysis made on the transverse microsections of the magnesium alloys using the EDS system have also confirmed the evident concentrations of magnesium, silicon, aluminium, manganese and iron what suggests the occurrence of precipitations containing Mg and Si with angular contours in the alloy structure as well as phases with high Mn and Al concentrations that are irregular with a non plain surface, often occurring in the forms of

blocks or needles(Figs. 7-8, Table 4), also information was obtained about the mass and atomic concentration of the particular elements in the point-wise investigated micro areas of the matrix and precipitates. Moreover the confirmation was achieved for alloying of Pb, Ce and Cu, identified in the γ phase area (Fig. 8, Table 4).
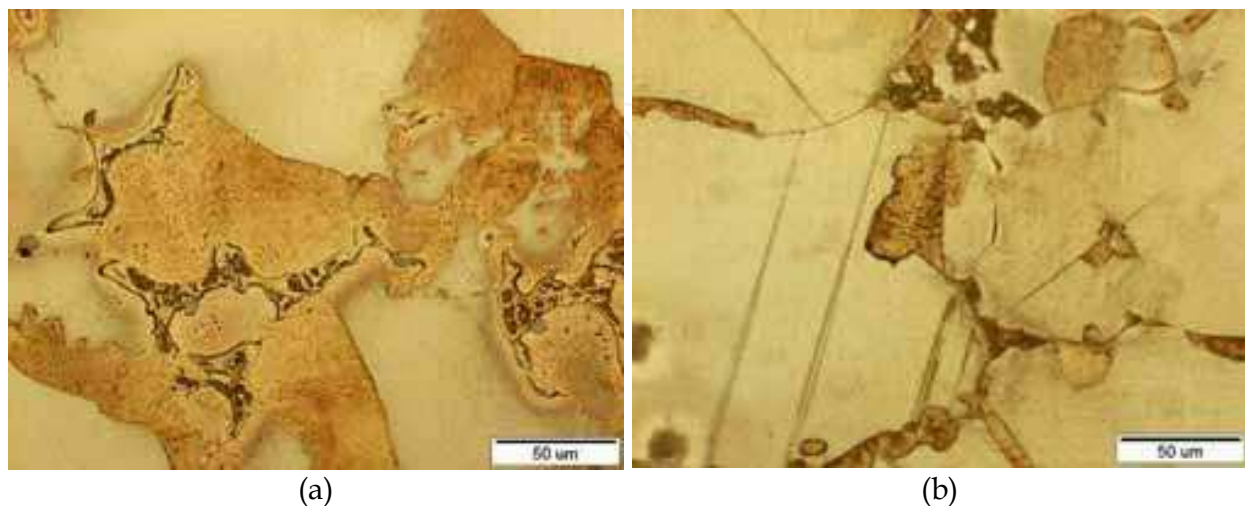

(a)   (b)

Fig. 6. Structure of the magnesium cast alloy: a) MCMgAl9Zn1 after cooling with the furnace; b) MCMgAl9Zn1 after ageing treatment

A prevailing participation of magnesium and aluminium and a slight concentration of Zn has been ascertained in the alloy matrix as well as in the location of eutectics and big precipitations that arouse at phase boundaries identified as $Mg_{17}Al_{12}$ (Fig. 7).

On Figure 9 there were presented X-Ray diffraction diagrams of the investigated magnesium alloys after heat treatment. Using qualitative and quantitative X-Ray diffraction methods it was confirmed, that in the investigated materials occurs the γ ($Mg_{17}Al_{12}$) phase and α-Mg phase - the alloy matrix. The volume fraction of the γ phase precipitation in the microstructure of the MCMgAl12Zn1, MCMgAl9Zn1, MCMgAl6Zn1 alloy depends on the aluminium content as the main alloying additive, with a maximum value of 11.9% for the MCMgAl12Zn1 alloy in the state after ageing - 1.6 % for the MCMgAl9Zn1 alloys in the state after ageing and MCMgAl6Zn1 alloy in the as-cast state. A to low volume fraction of other phases occurred in the material, as well the γ –$Mg_{17}Al_{12}$ phase for alloys after solution heat treatment or with a low aluminium content: MCMgAl9Zn1, MCMgAl6Zn1, MCMgAl3Zn1 does not allow for their clearly identification using the achieved X-Ray diagrams.

As a result of thin foils examinations on the transmission electron microscope it has been stated that the structure of a newly worked out, experimental magnesium cast alloy MCMgAl12Zn1, MCMgAl9Zn1, MCMgAl6Zn1, MCMgAl3Zn1 after solutioning makes a supersaturated solid solution α – Mg with visible dislocation ranges. The analysis of thin foils after the process of ageing has validated the fact that the structure of the magnesium cast alloy consists of the solid solution α – Mg (matrix) and an intermetallic secondary phase γ – $Mg_{17}Al_{12}$ in the form of bulk precipitations (Fig. 10).

Moreover, the examinations of the thin magnesium cast alloy foils after the ageing process confirm the existence of a high density of crystal structure defects identified as a series of straight and parallel dislocations resembling a network. The ageing process has caused the precipitation of evenly distributed dispersive γ secondary phase in the needle form that has in the major performed investigations a preferred crystallographic orientation in the matrix.
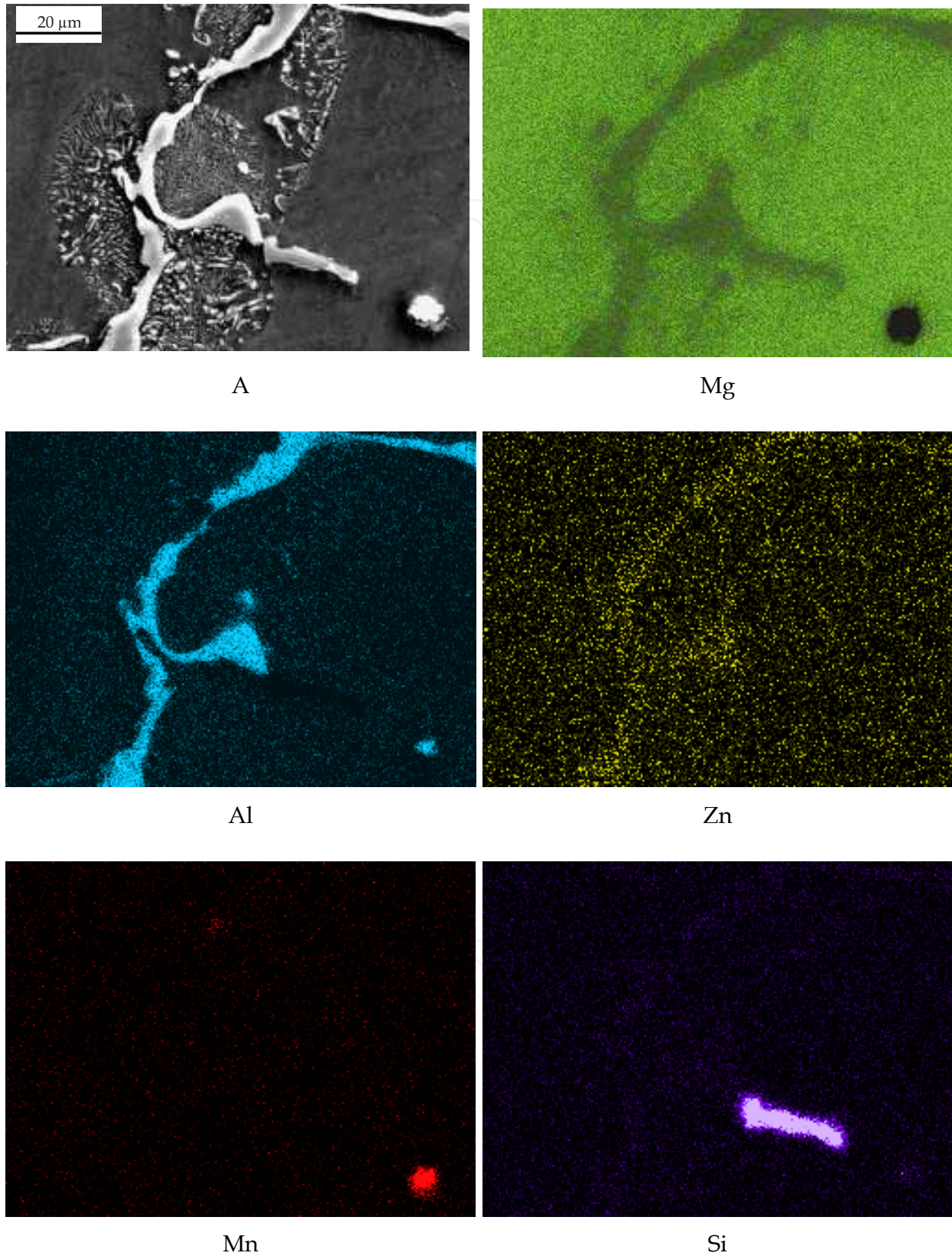
Fig. 7. The area analysis of chemical elements alloy MCMgAl6Zn1 after cooling in the furnace: image of secondary electrons (A) and maps of elements' distribution
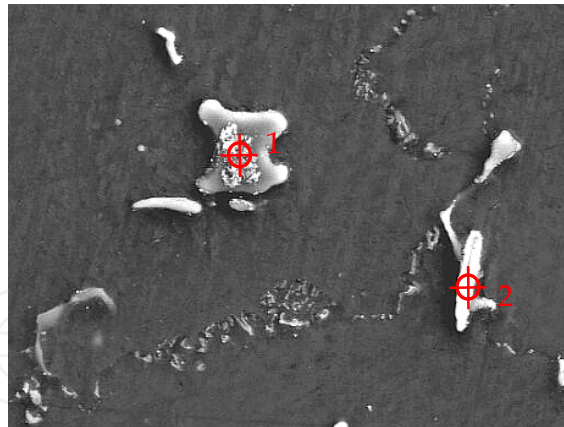
Fig. 8. Structure of the magnesium cast alloy MCMgAl6Zn1 after cooling in the furnace

Element	The mass concentration of main elements, %	
	Mass	Atomic
Analysis 1		
Mg	51.23	61.63
Al	24.36	29.25
Zn	5.54	5.23
Mn	0.11	0.06
Si	0.17	0.20
Fe	0.08	0.05
Cu	0.72	0.36
Pb	17.79	3.22
Analysis 2		
Al	50.32	60.88
Mn	37.05	34.53
Zn	0.78	0.28
Si	0.46	0.3
Fe	0.4	0.11
Cu	0.39	0.20
Pb	0.57	0.21
Ce	10.03	3.49

Table 4. Results of the quantitative analysis of chemical composition magnesium cast alloy MCMgAl6Zn1 after cooling in the furnace

According to the relations given by S. Guldberga and N. Ryuma (Guldberg and Ryum, 2000) which occured in the eutectic microstructure in the Mg alloys containing 33% Al. Some of the precipitations in the srudied magnesium alloys after solution heat treatment and ageing show an orientation, where the plains of the family {110} $Mg_{17}Al_{12}$ are rotated about 10° compared to the plains of the $\{1\bar{1}01\}$ family of the α - Mg solid solution, moreover other plains show bigger rotation value as given by S. Guldberga and N. Ryuma (Guldberg and Ryum, 2000). Precipitation of the γ - $Mg_{17}Al_{12}$ phase are mostly of the shape of roads, and the prevailing growing directions are the directions $\langle 110 \rangle$ α - Mg (Figs. 10,11).
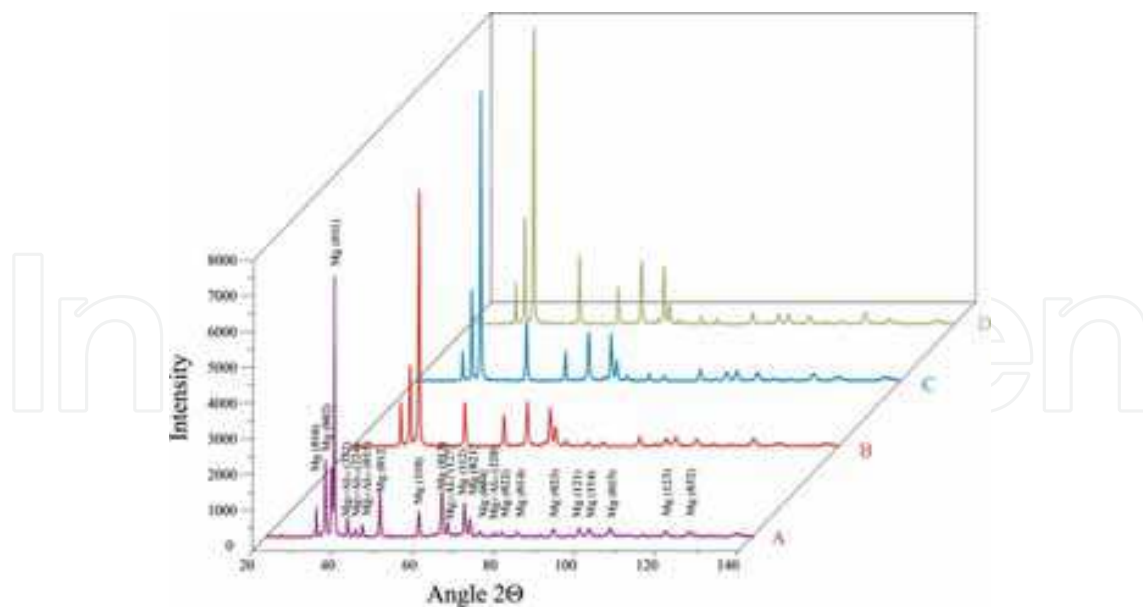
Fig. 9. X ray diffraction pattern of the magnesium cast alloys: A - MCMgAl12Zn1,
B - MCMgAl9Zn1, C - MCMgAl6Zn1, D - MCMgAl3Zn1 after ageing treatment

A part of them shows the following relation (Fig. 10):

$$(1\bar{1}01)\alpha\text{-Mg}\|(10\bar{1})\text{Mg}_{17}\text{Al}_{12}$$
$$[11\bar{2}0]\alpha\text{-Mg}\|[111]\text{Mg}_{17}\text{Al}_{12}$$

Influence of the aluminium content and heat treatment on properties of the cast magnesium alloys are presented on Fig. 12. Hardness increases together with the increase of aluminium content in the analyzed alloys from 3 to 12%. The highest hardness of 75 HRF in as cast state occurs in case of the MCMgAl12Zn1 alloy casts. This value is about two times higher compared to the MCMgAl3Zn1 alloy with a value of 30 HRF. Heat treatment applied on the material (solution heat treatment and ageing) causes a hardness increase. The MCMgAl12Zn1, MCMgAl9Zn1 and MCMgAl6Zn1 alloys have reach the highest hardness after ageing, adequately 94, 75 and 53 HRF and after solution heat treatment and cooling with furnace 85, 71 and 52 HRF. For cases after solution heat treatment hardness slightly decreases compared to the initial state. For MCMgAl3Zn1 casts the highest hardness have the samples after ageing and cooling in water - 41 HRF, for other cases the hardness values are similarly to each other.

The influence of aluminium content and heat treatment on the tensile strength of the cast magnesium alloys was showed on Figures 13 and 14. Results of the tensile strength test allows it to determine and compare the mechanical properties of the investigated cast magnesium alloys in as cast state and after heat treatment applied. On the basis of the performed investigations it was state, that the highest tensile strength in as cast state is characteristic for the MCMgAl6Zn1 and MCMgAl3Zn1 alloy - 192.1 and 191.3 MPa respectively, theses alloys have also the highest elongation value in as cast state – 11.6 and 15.2 %.

It was showed, that the increase of aluminium content from 6 to 12 % decreases the tensile strength in as cast state to the value of 170.9 MPa. Heat treatment like solution heat treatment and cooling with furnace causes increase of tensile strength (Fig. 13).
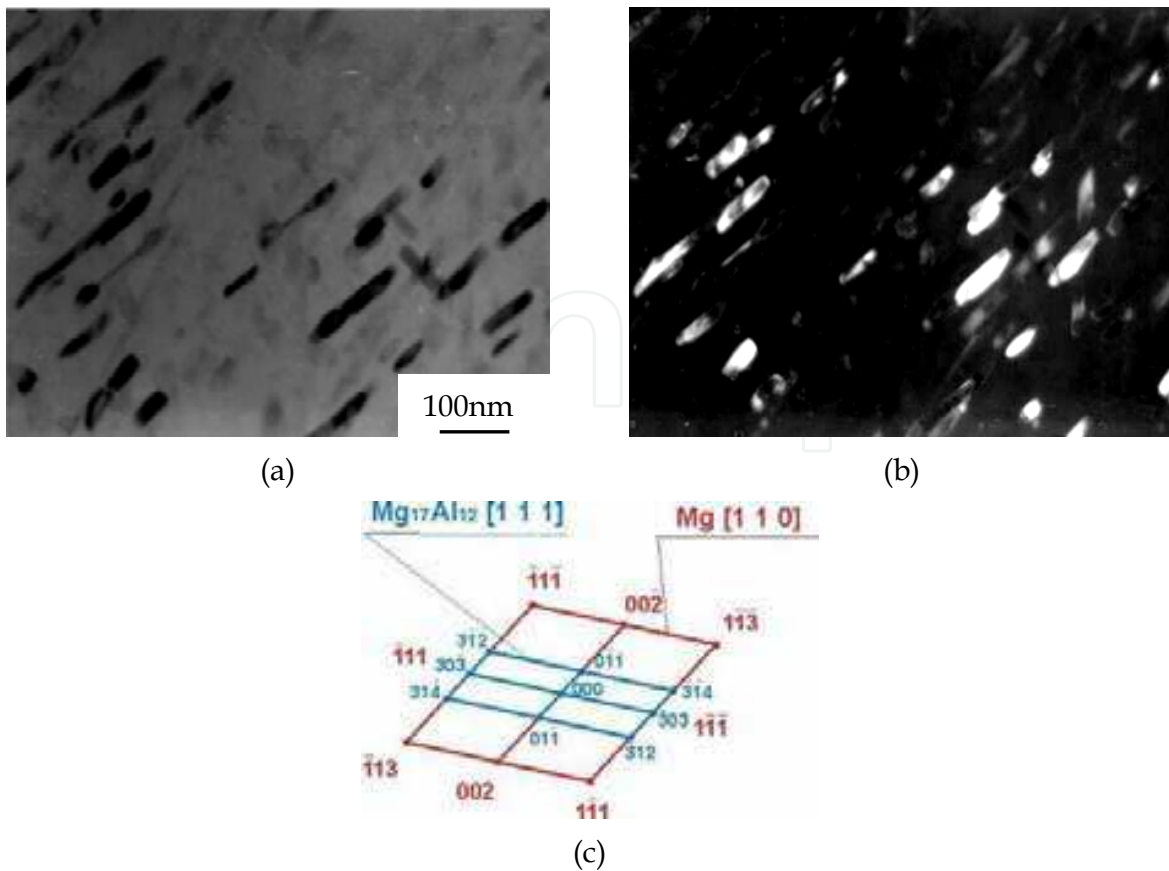
(a)   (b)

(c)

Fig. 10. a), b) Bright and dark field (with spot ($\overline{3}1\overline{4}$)) image of the MCMgAl9Zn1 alloy after aging treatment with solid solution α – Mg (matrix) and an intermetallic secondary phase γ – $Mg_{17}Al_{12}$ in the form of needle precipitations, c) diffraction pattern of area shown in a), d) part of solution for diffraction pattern shown in c
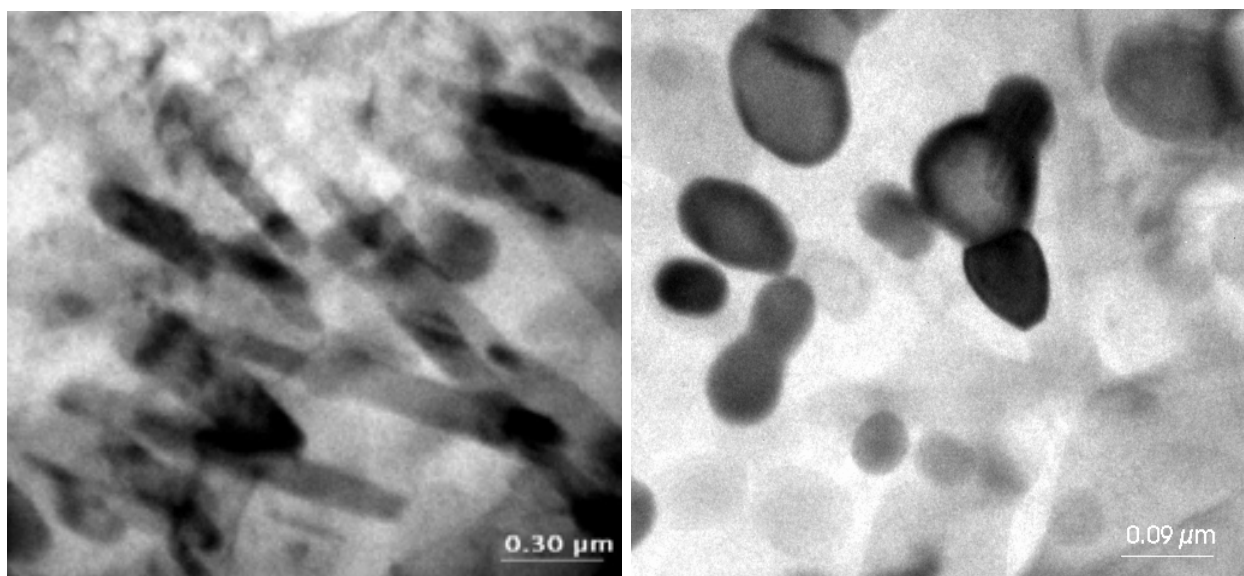

Fig. 11. TEM image examples of the intermetallic secondary phase γ – Mg17Al12 in the form of needle precipitations from the MCMgAl9Zn1 alloy after aging treatment
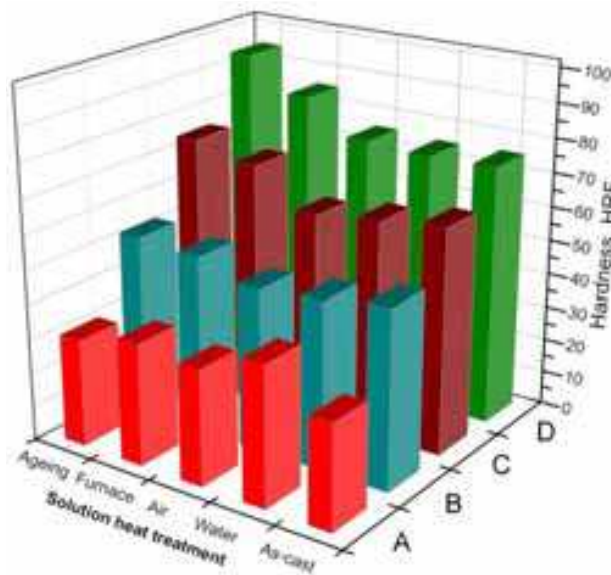
Fig. 12. Results of HRF hardness measurements of magnesium cast alloys: A –MCMgAl3Zn1, B – MCMgAl6Zn1, C – MCMgAl9Zn1, D – MCMgAl12Zn1
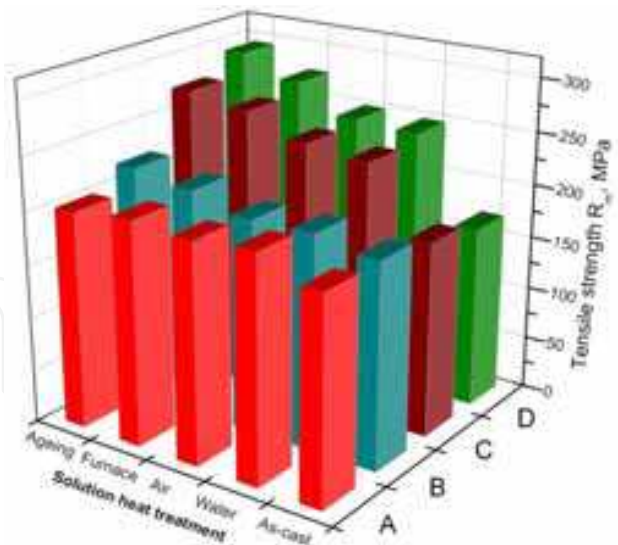

Fig. 13. Results of tensile strength Rm measurements of magnesium cast alloys: A – MCMgAl3Zn1, B – MCMgAl6Zn1, C – MCMgAl9Zn1, D – MCMgAl12Zn1
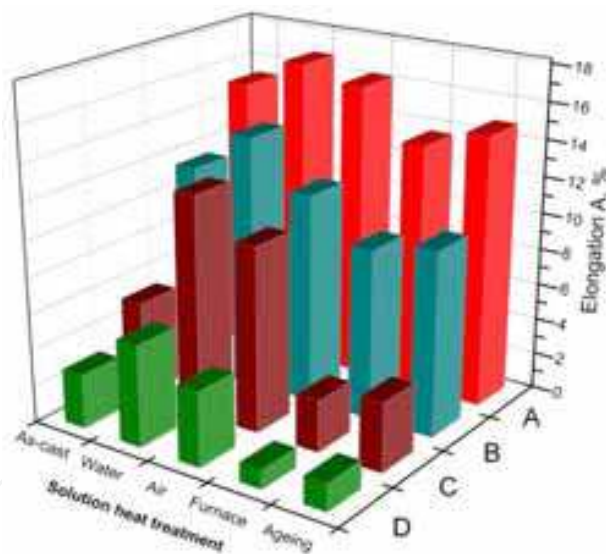

Fig. 14. Results of elongation A measurements of magnesium cast alloys: A – CMgAl3Zn1, B – MCMgAl6Zn1, C – MCMgAl9Zn1, D – MCMgAl12Zn1

3.2 Thermal analysis

An example of the cooling and crystallization curve of the Mg-Al-Zn alloy cooled with different cooling rates are presented on Figure 15. The performed crystallization process analysis on the basis of the achieved curves allows it to state, that the nucleation process of the α phase begins at the T_{DN} temperature. This effect is present on the curve in form of an inflexion in point I, as well in form of an instantaneous decrease of the cooling rate. Decrease of the crystallisation rate of the remaining liquid metal is caused by the heat provided from the α phase nuclei, which is smaller compared to the heat amount submit into the

surrounding by the solidified metal. This process ends in point II, where the crystallization temperature achieves the minimal value - T_{Dmin}, where the α phase crystals begins to growth. In this point the derivative value achieves the zero value. The cooled alloy, resulting in crystallisation heat emission, reheats the remaining liquid until the T_{DKP} (point III) temperature. The further crystal growth causes an increase of the temperature of the remaining liquid to the maximal crystallisation temperature of the α phase – T_G (point IV). Further alloy cooling causes the beginning of crystallisation of the silicon, aluminium and manganese- rich phases, which are emitting an additive heat amount present on the crystallisation curve in form of clear heat effect – described as $T_{(Mg+Si+Al+Mn)}$ and $T_{(Mg+Si+Al+Mn)f}$ (points V and VI). As a result of further alloy cooling after reaching the $T_{E(Mg+Al)N}$ temperature there occurs the nucleation of the α+γ eutectic (point VII). The cooled alloy reach the $T_{E(Mg+Al)min}$ (point VIII) temperature, as next the temperature increases until the maximum crystallisation temperature of the eutectic $T_{E(Mg+Al)G}$ (point IX). The alloy crystallisation ends in point X, where the T_{sol}. Value is reached. In Table 5 there is presented ten crystallisation temperature of the particular phases as well the solid state fraction for a chose example.

On Figure 17 there is presented the solid state fraction change as well the heat flux generated by the crystallised phases. This information is used for determination of the crystallising heat emitted by the particular phases (Table 6). On Figure 17 there is also presented the influence of the cooling rate as well the magnesium content on the temperature - T_{DN} of the *a* phase nucleation. On the basis of the performed investigation it was found that the biggest influence on the nucleation temperature has the aluminium content (it decreases the nucleation temperature of the *a* phase according to the liquidus line) as well the cooling rate (it causes an increase of the *a* phase nucleation temperature). For example for the MCMgAl3Zn1 alloy an increase of the cooling rate from 0.6 to 1.2°C/s causes an increase of the *a* phase nucleation temperature from 633.16 to 635.39°C, further increase of the cooling rate until 2.4°C/s causes a temperature growth until 640.32°C.

On Figure 18 there is presented the influence of the magnesium mass concentration as well the cooling rate on the maximal crystallisation temperature (T_G) of the *a* phase. On the basis
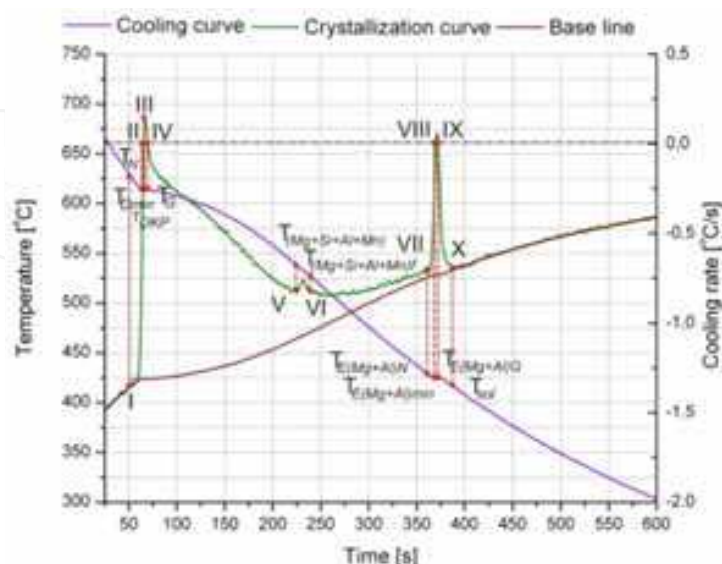

Fig. 15. Representative cooling, crystallization and calorimetric curves with characteristics points of crystallization process of MC MgAl6Zn1 alloy cooled at 0.6°C/s

Temperature, T; time, t; fraction solid, f_s	Avarage	Confidence interval		Standard deviation	Error, %
		-95%	+95%		
T_{DN}	615.88	611.66	620.09	3.40	0.55
T_{Dmin}	611.51	609.12	613.91	1.93	0.32
f_s	1.96	1.35	2.57	0.49	24.96
T_{DKP}	611.75	609.34	614.16	1.94	0.32
f_s	3.16	2.42	3.9	0.6	18.86
T_G	611.92	609.45	614.39	1.99	0.33
f_s	5.44	4.35	6.52	0.87	16.07
$T_{(Mg+Si+Al+Mn)}$	533.65	527.69	539.62	4.81	0.9
f_s	85.28	82.83	87.73	1.97	2.31
$T_{(Mg+Si+Al+Mn)f}$	520.18	513.3	527.05	5.54	1.06
f_s	88.08	85.74	90.42	1.89	2.14
$T_{E(Mg+Al)N}$	429.45	426.56	432.34	2.33	0.54
f_s	95.02	93.84	96.21	0.95	1.00
$T_{E(Mg+Al)min}$	426.59	423.81	429.36	2.23	0.52
f_s	96.03	94.72	97.34	1.05	1.10
$T_{E(Mg+Al)G}$	427.17	424.08	430.27	2.49	0.58
f_s	97.96	97.39	98.53	0.46	0.47
T_{sol}	419.47	415.42	423.52	3.26	0.78

Table 5. Thermal characteristic of MCMgAl6Zn1 alloy cooled at 0.6°C/s

Specific heat in liquid state Cp_l, J/g·°C	Specific heat in solid state Cp_s, J/g·°C		Weight, g
1.21	1.01		8.99
Reaction	Latent heat of crystallization process		Participation, %
	Per sample, J	Per 1 gram of sample, J/g	
L→ α(Mg)	1258.22	139.96	86.31
L→ α(Mg)+Mg$_2$Si+(Al+Mn)	143.63	15.98	9.85
L→ α(Mg)+γ(Mg$_{17}$Al$_{12}$)	55.98	6.23	3.84
Razem	1457.84	162.16	100

Table 6. Latent heat of crystallization emitted during solidification and its participation in general latent heat of MC MgAl6Zn1 cooled at 0.6 °C/s

Fig. 16. Representative curves illustrate changes of heat flux and fraction solid of
MCMgAl6Zn1 alloy MCMgAl6Zn1 cooled at 0.6°C/s

of the performed investigation it was found that the change of the cooling rate does not
influence the maximal crystallisation temperature (T_G) of the *a* phase. It was also found that
the T_G temperature decreases together with the increase of the aluminium content. For
example for the alloys cooled with a rate of 0.6°C/s, the increase of aluminium content from
3 to 6% causes a decrease of the maximal crystallisation temperature of the *a* phase from
630.85 to 611.92°C, and a further increase of the aluminium content of 9% causes a decrease
of the temperature value to 592.91°C. The lowest values of the maximal *a* phase
crystallisation temperature - equal 576.03°C, was observed for the alloy with 12%
aluminium content.

Fig. 17. Influence of cooling rate on Mg_{Den}
nucleation temperature (T_{DN}):
A – MCMgAl3Zn1, B – MCMgAl6Zn1,
C – MCMgAl9Zn1, D – MCMgAl12Zn1

Fig. 18. Influence of cooling rate on Mg
dendrite growth temperature (T_G):
A – MCMgAl3Zn1, B – MCMgAl6Zn1,
C – MCMgAl9Zn1, D – MCMgAl12Zn1

On Figure 19 there is presented the influence of cooling rate as well the influence of aluminium mass content on the heat amount emitted during the alloy crystallisation. On the basis of the performed calculations it was found, that the biggest influence on the heat (Q_c) increase generating during alloy crystallisation has the variable aluminium content. An increase of thee aluminium content in the investigated alloys causes an increase of the heat Q_c. In case of an increase of the cooling rate there was observed a small growth of the generating crystallisation heat except the MCMgAl3Zn1 alloy.

The carried out investigations revealed, that the grain size decreases together with the cooling rate increase for each of the analysed alloys. On the basis of the performed investigations it was found that the largest grain size is characteristic for the MCMgAl6Zn1 alloy (Table 7). A cooling rate change from 0.6 to 2.4°C/s causes a two times decrease of the grain size. A similar dependence was found also for other analysed alloys, which were studied in this investigation. An increase of the aluminium mass concentration causes a slightly decrease of the grain size (Fig. 20).

Figure 21 shows the influence of aluminium mass concentration as well the cooling rate on hardness of the investigated alloys. On the basis of the performed investigations it was found a linear increase of the hardness compared to the increase of the aluminium content, and also an increase of the cooling rate for the MCMgAl6Zn1, MCMgAl9Zn1 and MCMgAl12Zn1 alloy. For the MCMgAl3Zn1 alloy it was found a hardness increase up to 26 HRF by a cooling rate of 1.2°C/s. A cooling rate increase up to 2.4°C/s causes a decrease of the hardness down to 19 HRF. The highest hardness value of 74 HRF was achieved for the MCMgAl12Zn1 alloy cooled with a rate of 2.4°C/s.

Figure 22 presents the influence of aluminium mass concentration as well the cooling rate on the ultimate compressive strength. On the basis of the performed investigations it was found that the highest value of the ultimate compressive strength of 296.7 MPa has the MCMgAl6Zn1 alloy, and the lowest value of 245.9 MPa the MCMgAl3Zn1 alloy (both alloys cooled with a rate of 0.6°C/s). A change of the cooling rate of the analysed alloys causes an increase of the ultimate compressive strength. The highest increase of the R_c value in
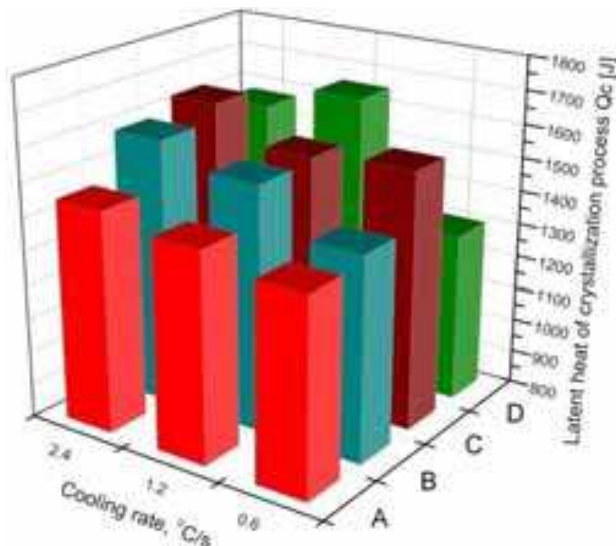

Fig. 19. Influence of cooling rate on latent heat of crystallization process:
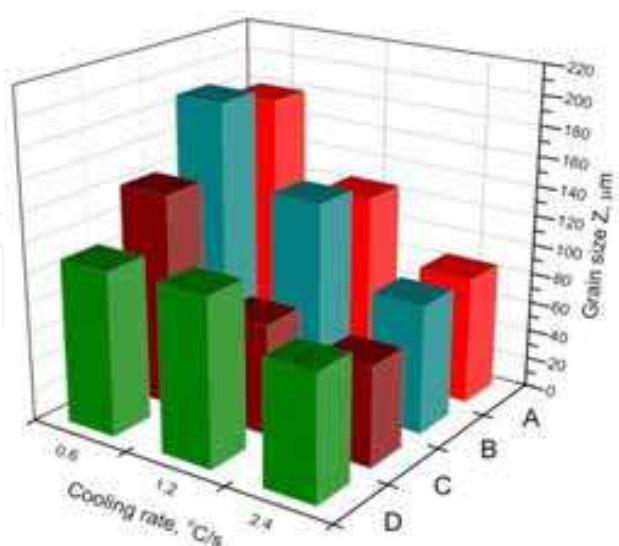A – MCMgAl3Zn1, B – MCMgAl6Zn1,
C – MCMgAl9Zn1, D – MCMgAl12Zn1

Fig. 20. Influence of cooling rate on grain size: A – MCMgAl3Zn1, B – MCMgAl6Zn1, C – MCMgAl9Zn1, D – MCMgAl12Zn1

comparison to the cooling rate increase was found in case of the MCMgAl3Zn1 and MCMgAl9Zn1 alloy. An increase of the cooling rate up to the maximum value causes an increase of the ultimate compressive strength for the MCMgAl3Zn1 and MCMgAl9Zn1 alloy up to the value of 275.8 and 316 MPa adequately, as well is ca. 10-15 MPa higher in case of the MCMgAl6Zn1 and MCMgAl12Zn1 materials.

Alloy	Cooling rate, °C/s	Grain size Z, µm	Confidence interval		Standard deviation	Error, %
			-95%	+95%		
MCMgAl3Zn1	0.6	179.26	154.38	204.14	20.04	11.18
	1.2	125.48	115.20	135.75	8.28	6.6
	2.4	85.4	77.11	93.68	6.67	7.82
MCMgAl6Zn1	0.6	190.3	177.87	202.74	10.01	5.26
	1.2	137.05	123.54	150.56	10.88	7.94
	2.4	86.28	80.27	92.29	4.84	5.61
MCMgAl9Zn1	0.6	143.53	114.83	172.24	23.12	16.11
	1.2	74.46	59.24	89.69	12.26	16.47
	2.4	66.73	52.8	80.66	11.22	16.82
MCMgAl12Zn1	0.6	110.39	83.01	137.76	22.05	19.97
	1.2	112.26	109.59	114.94	2.15	1.92
	2.4	84.58	74.73	94.44	7.94	9.39

Table 7. Grain size of MCMgAl3Zn1, MCMgAl6Zn1, MCMgAl9Zn1, MCMgAl12Zn1 cooled with different cooling rates
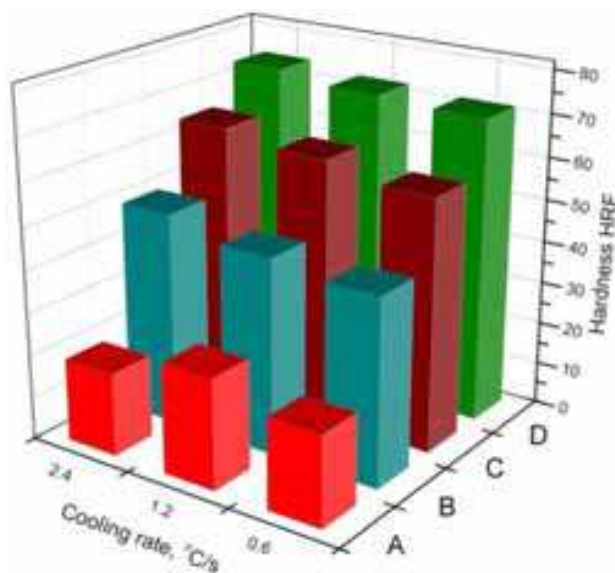
Fig. 21. Influence of coolng rate on hardness: A – MCMgAl3Zn1, B – MCMgAl6Zn1, C – MCMgAl9Zn1, D – MCMgAl12Zn1
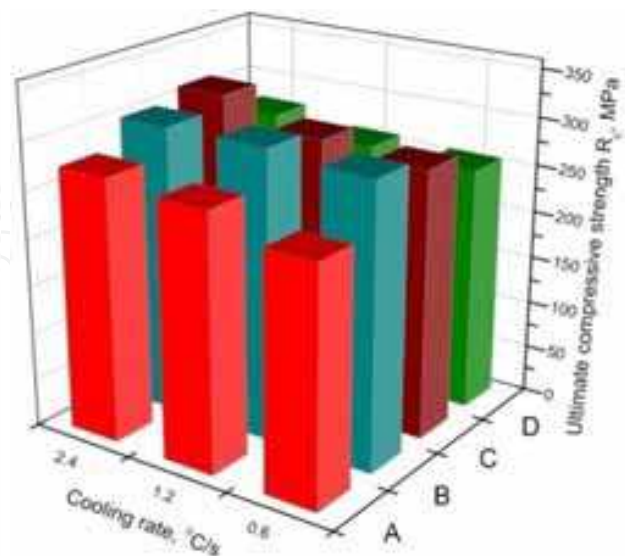
Fig. 22. Influence of coolng rate on ultimate compressive strength R_C: A – MCMgAl3Zn1, B – MCMgAl6Zn1, C – MCMgAl9Zn1, D – MCMgAl12Zn1

3.3 Laser treatment

The shape of the laser face performed on the MCMgAl3Zn1, MCMgAl6Zn1, MCMgAl9Zn1, MCMgAl12Zn1 cast magnesium alloy after laser alloying with carbides and aluminium oxide using high power diode laser HPDL is presented on Figure 23. It was found a clearly influence of the process parameters, particularly power of the laser beam as well ceramic powders used on the shape and topography of the surface. The laser face, after alloying with the TiC and WC powders using the feeder is characterised by a regular, flat surface (Fig. 23a, b). In case of vanadium carbide the laser face is characterised by a flat shape of the remelting area, however with visible discontinuities of the surface layer. The investigated material after SiC powder alloying is characterised by a clear relief of the remelting area standing over the surface level of the non remelted material (Fig. 23c). After NbC powder remelting, the surface layer of the cast magnesium alloys is characterised by very irregular surface and some break flows of the material present outside of the laser face. Where as the appliance of Al_2O_3 powder causes some small hollows in the middle of the lacer face in case of 2.0 kW laser power. On Figure 23d there is presented the laser face of the MCMgAl3Zn1 cast magnesium alloy after alloying with Al_2O_3 powder using 1.6 laser power, where the laser treatment was interrupt. Investigations reveal, that the laser power increase by a stable laser beam scanning rate influences the size of the remelting area , where some structural changes occur in the surface layer of the Mg-Al-Zn alloys. The power of the laser beam is also related

(a) (b) (c) (d)
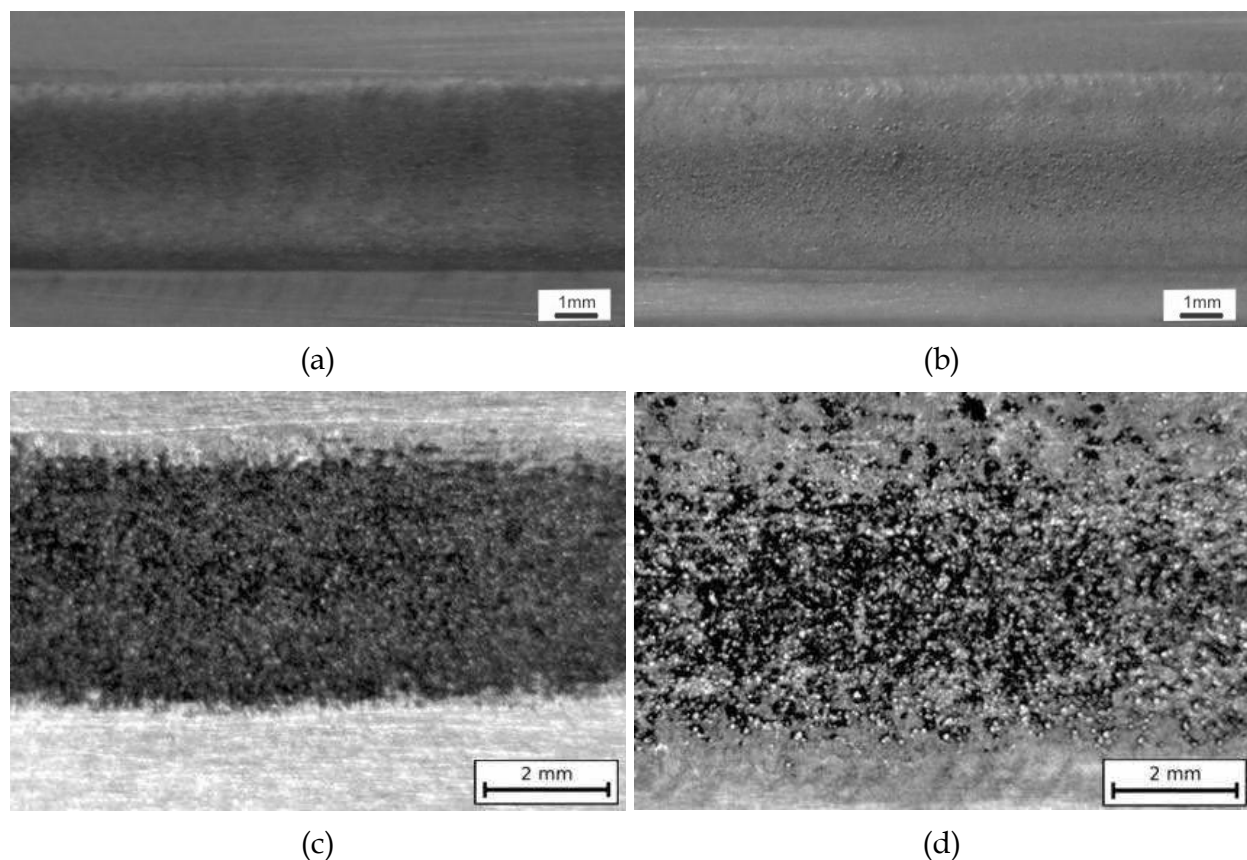
Fig. 23. Surface layer face of the magnesium cast alloy: a) MCMgAl3Zn1 alloyed with TiC, laser power 1.2 kW, alloying speed 0.75 m/min; b) MCMgAl3Zn1 alloyed with WC, laser power 1.6 kW, alloying speed 0.75 m/min; c) MCMgAl3Zn1 alloyed with SiC, laser power 1.6 kW, alloying speed 0.75 m/min; d) MCMgAl12Zn1 alloyed with Al_2O_3, laser power 2.0 kW, alloying speed 0.50 m/min

to the shape of the bottom of the remelting area as well the convexity of the laser face, which depends also on strong liquid metal movements during the remelting process.

On the basis of roughness measurements of the surface of the cast magnesium alloys after laser alloying with the titanium, tungsten, vanadium, silicon and aluminium oxide (Fig. 24) it was state, that apart from the applied ceramic powder, the roughness of the surface layers abstained by laser remelting of the Mg-Al-Zn alloys with a power in the range of 1.2 ÷ 2.0 kW increases and reach a value in the range of R_a = 6.4 – 42.5 µm.

For each type of substrate (independent of the aluminium content) the highest roughness have the samples after laser alloying by a scanning rate of 0.5 m/min with laser power of 2.0 kW. By a stable scanning rate and a not changed powder feeding, together with an increase of the laser power the surface roughens decreases. Among the investigated Mg-Al-Zn cast magnesium alloys the lowest roughness respectively 4.0 and 5.6 µm have the MCMgAl9Zn1 and MCMgAl12Zn1 materials after alloying with VC powder, by applied laser power of 2.0 kW. A maximal measured surface roughness of R_a = 42.5 µm occurs in case of the surface layer of the MCMgAl9Zn1 alloy after laser alloying with SiC powder with laser power of 1.2 kW. The investigated material after alloying with titanium carbide powder are characterised by a roughness in the range of 6.4-13.9 µm. In case of vanadium carbide powder it was found, that the highest roughness value, by a stable scanning rate of 0.75 m/min, for each type of alloy, have the samples after alloying with 1.2 kW laser power, whereas the highest roughness value has the MCMgAl3Zn1 alloy by applied laser power of 1.2 kW (25.43 µm). An increase of the irregularity of the surface after laser treatment is related to the fluctuation of the alloyed material caused by changes of the remelting material tensions as well the laser beam energy absorbed by the alloyed material.
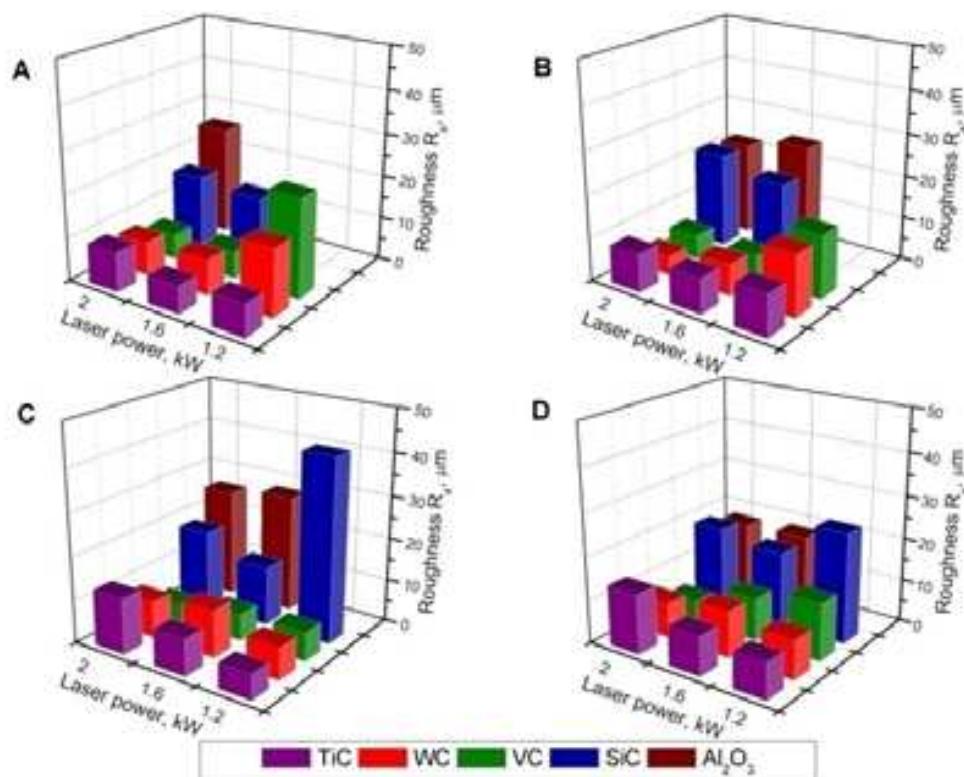

Fig. 24. Laser power and Al mass concentration influence on roughness of alloyed surface layer: A – MCMgAl3Zn1; B – MCMgAl6Zn1 ; C – MCMgAl9Zn1; D – MCMgAl12Zn1

On Figure 25 there is presented the zone placement on the cross section of the remelting laser face of the Mg-Al-Zn cast magnesium alloys. On the basis of the performed metallographic investigations it was found, that in each of the surface layer after surface laser treatment of the MCMgAl12Zn1 and MCMgAl9Zn1 cast magnesium alloys occur a remelting zone (RZ) as well a heat affected zone (HAZ). These zones, depending on the laser power as well the ceramic powder used have a different thickness and shape. In case of the TiC, WC and VC powder for the MCMgAl6Zn1 alloy it was found a very small HAZ, which increases together with the laser power applied. In case of alloying of the ceramic powder into the surface of the MCMgAl3Zn1 alloys there is present only the remelting zone as well the boundary between the remelting zone and the material substrate. On the basis of the performed investigations it is possible to state that the change of the laser power by a constant alloying rate clearly influences the thickness of both zones in the surface layer. The applied laser power influences also the shape and the convexity of the remelting zone (Fig. 25), which reach over the surface of the untreated material.

(a)   (b)

(c)   (d)
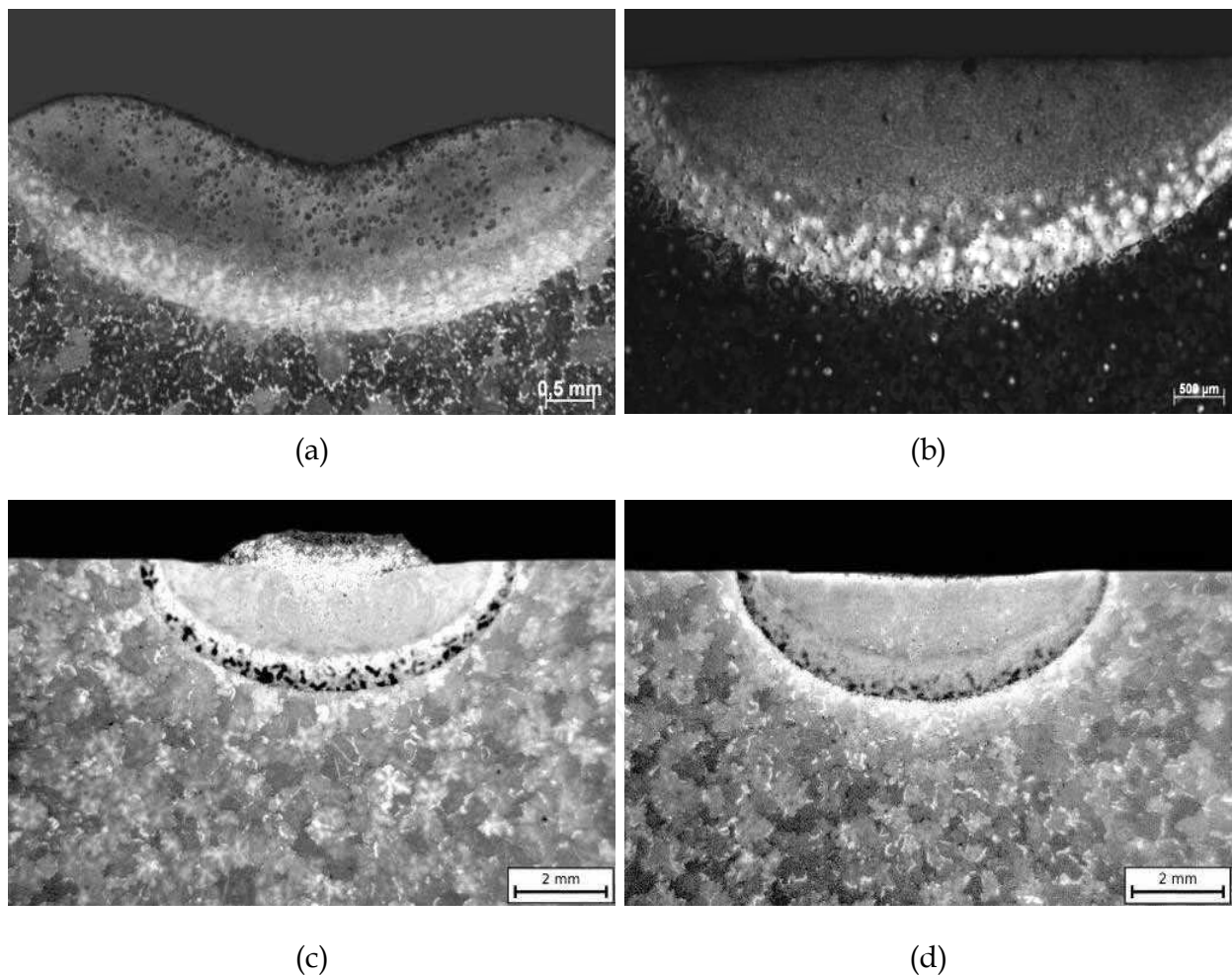
Fig. 25. Surface layer of the magnesium cast alloy: a) MCMgAl9Zn1 alloyed with TiC, laser power 1.2 kW, alloying speed 0.75 m/min; b) MCMgAl9Zn1 alloyed with WC, laser power 1.2 kW, alloying speed 0.75 m/min; c) MCMgAl12Zn1 alloyed with SiC, laser power 2.0 kW, alloying speed 0.75 m/min; d) MCMgAl12Zn1 alloyed with Al_2O_3, laser power 2.0 kW, alloying speed 0.50 m/min

Results of the metallographic investigations show that the structure of the solidified material after laser alloying is characterised by the occurrence of areas with different morphology connected to the crystallisation of the magnesium alloys (Fig. 26). As a result of the laser alloying a structure is achieving which is free of defects and with a clear grain refinement. The structure of the laser modified layer contains mainly dispersive particles of the applied carbide powder TiC, WC, VC, SiC, NbC or Al_2O_3 oxide placed in the matrix of the Mg-Al-Zn alloy.

Morphology of the treated area after laser alloying is mainly compound of dendrites wit plate shaped $Mg_{17}Al_{12}$ eutectic and Mg present in the interdendritic space, where the main growing axes are directed according to the heat transport directions. This can be interpret with a occurrence of a non-normal eutectic with a small amount of α-Mg in the eutectic solution. Moreover the composite structure of the area after laser treatment results from the hypo-eutectic alloy change to a hyper-eutectic one, depending from the alloyed elements distribution and the change of the process condition parameters of the laser treated surface.

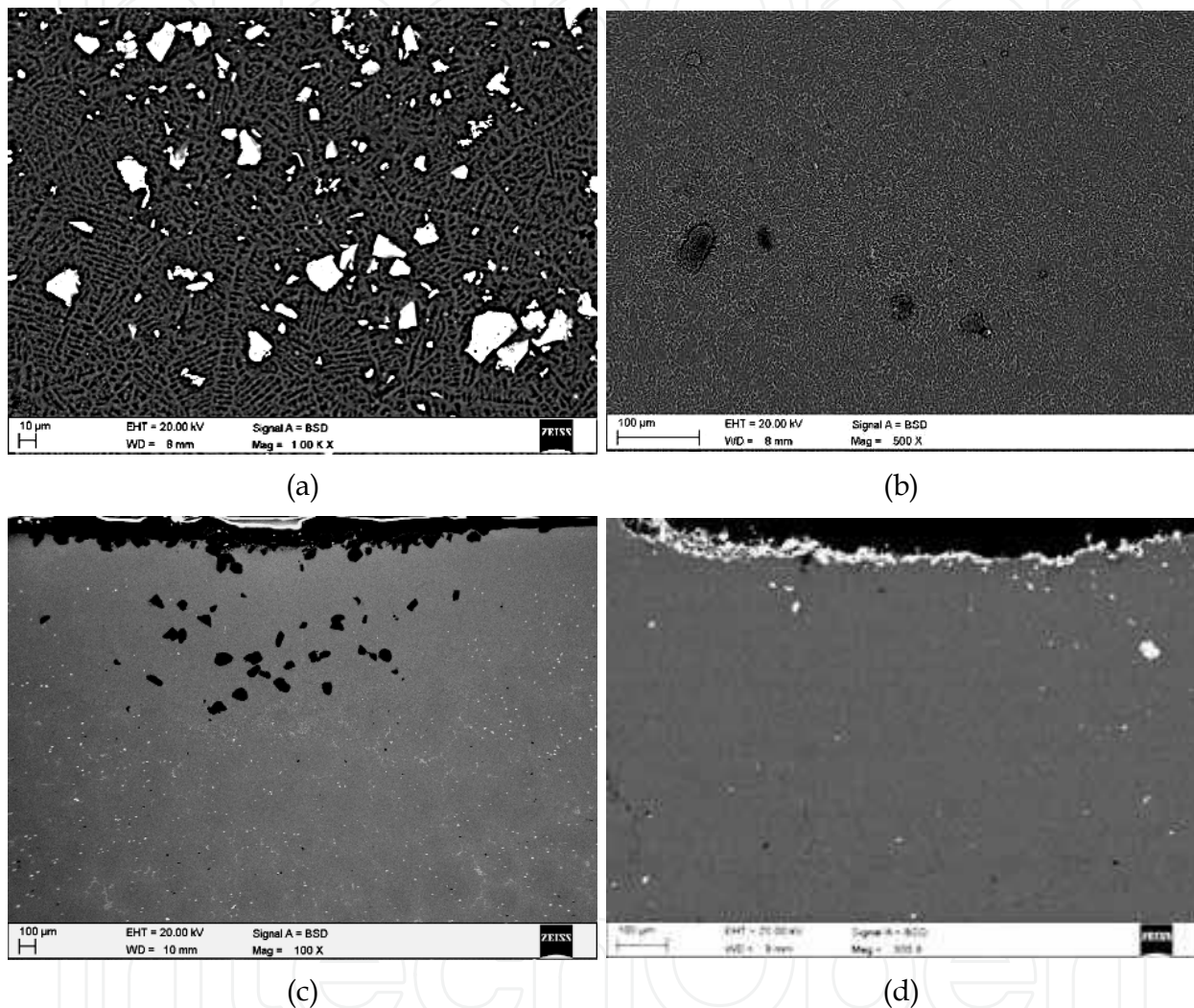(a)   (b)
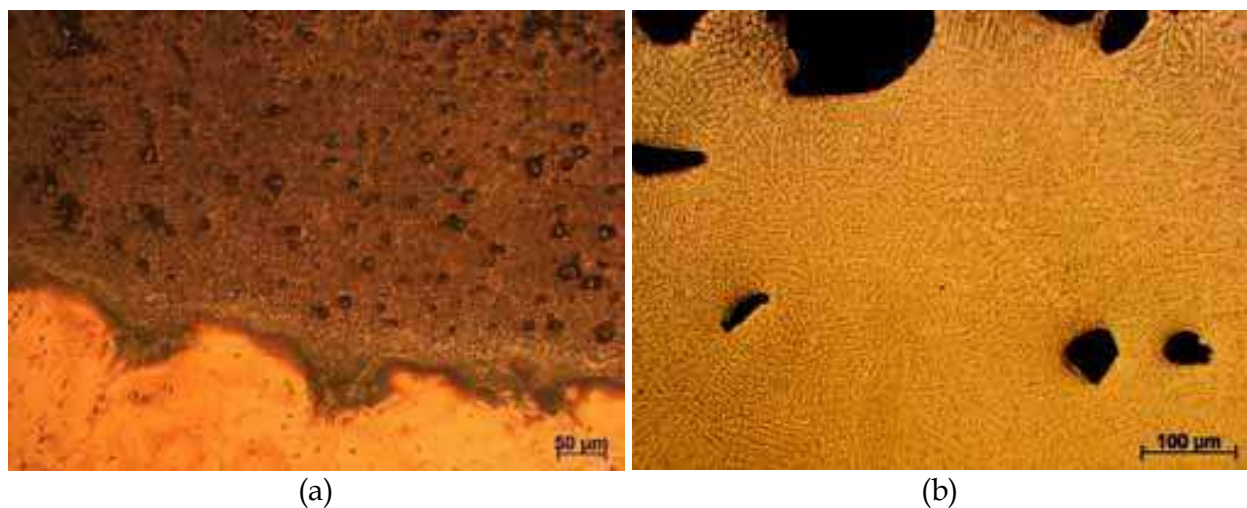
Fig. 26. Microstructure of the: a) edge of remelted zone of MCMgAl6Zn1 alloyed with TiC, laser power 1.6 kW, alloing speed 0.75 m/min; b) middle of surface layer of MCMgAl3Zn1 alloyed with Al2O3, laser power 2.0 kW, alloying speed 0.50 m/min

Investigations carried out on the scanning electron microscope confirm the occurrence of the zones in the surface layer of the investigated cast magnesium alloys (Fig. 27). In the remelted zone there is present a dendritic structure build according to the heat transport directions, there are also present the alloyed powder particles of the carbides or aluminium oxide. The morphology after surface laser treatment, including the amount and distribution of the carbide particles, depends on the applied laser parameters. On the basis of the metallographic investigations of the MCMgAl3Zn1, MCMgAl6Zn1, MCMgAl9Zn1, MCMgAl12Zn1 alloys it was found a uniform distribution - on the whole remelting zone – of the used carbide particles TiC, WC and Al_2O_3. (Fig. 27a, c). In case of alloying of the SiC particles with laser power of 1.2 kW, the carbides are mainly located on the top of the surface layer. For power of 2.0 and 1.6 kW in samples of the MCMgAl12Zn1 and MCMgAl9Zn1 material, caused by a strong movement of the liquid metal in the melting area, the SiC particles are distributed over the whole area of the remelting zone. After alloying with vanadium carbide in the surface of the cast magnesium alloys there was observed only a sporadically occurrence of the carbide in the remelting area (Fig. 27b). A

similar regularity was found in case of niobium carbide, the alloyed material was not revealed in the structure of the remelting zone or was found near the top of the surface of the composite layer (Fig. 27d). In cast magnesium alloys alloyed with NbC powder there were found small cracks and breaks in the surface layer of the material.

X-Ray diffraction diagrams of Mg-Al-Zn cast magnesium alloys after laser alloying with WC, TiC, VC, SiC carbides and Al_2O_3 oxide confirm the occurrence of α – Mg phase, γ – $Mg_{17}Al_{12}$ phase, as well of picks coming from the powders using for alloying (Fig. 28).

(a)   (b)

(c)   (d)

Fig. 27. Microstructure of the : a) middle of remelted zone of MCMgAl3Zn1 alloyed with TiC, laser power 1.2 kW, alloying speed 0.75 m/min; b) middle of remelted zone of MCMgAl12Zn1 alloyed with VC, laser power 1.6 kW, alloying speed 0.75 m/min; c) surface layer of MCMgAl9Zn1 alloyed with Al_2O_3, laser power 2.0 kW, alloying speed 0.50 m/min; d) surface layer of MCMgAl6Zn1 alloyed with NbC, laser power 2.0 kW, alloying speed 0.25 m/min

Line EDS analysis as well the area EDS analysis of the elements distribution on cross-section of the surface layer of laser treated Mg-Al-Zn cast magnesium alloys using TiC, WC, VC, SiC and Al_2O_3 powders confirm the occurrence of magnesium, aluminium, zinc, manganese, carbide, as well respectively titanium, tungsten, vanadium, silicon, as well

oxygen in the laser modified surface layer, the results reveal also a lack of occurrence of the alloyed particles.

On the basis of the results achieved from thin foils investigation of the cast magnesium alloys after laser alloying of TiC and WC powder it was confirmed the occurrence of the TiC (Fig. 29) and WC (Fig. 30).

The micro hardness test results performed on cross-section of the laser face measured in function of the distance from surface are presented on Figure 31. The substrate material is characterised by a hardness in the range of 50 $HV_{0,1}$ to 100 $HV_{0,1}$, whereas the remelting zone has a hardness in the range 150 to 700 $HV_{0,1}$. The performed investigation show, that the micro hardness decreases with the distance from the top to the substrate direction, which is probably cussed by a fine grained structure in the top of the surface layer as well by the occurrence of hard carbides used for alloying. In some areas there occur some significant differences in the precision of measurements, probably caused by an irregular distribution of the hard particles.

Micro hardness of the MCMgAl6Zn1 cast magnesium alloys in the heat affected zone is similar to the micro hardness value of the substrate material after laser treatment (Fig. 31a,b), whereas in case of the MCMgAl12Zn1 and MCMgAl9Zn1 alloys there was found a decrease of the micro hardness in the heat affected zone which is below the value of the substrate material (Fig. 31c,d).
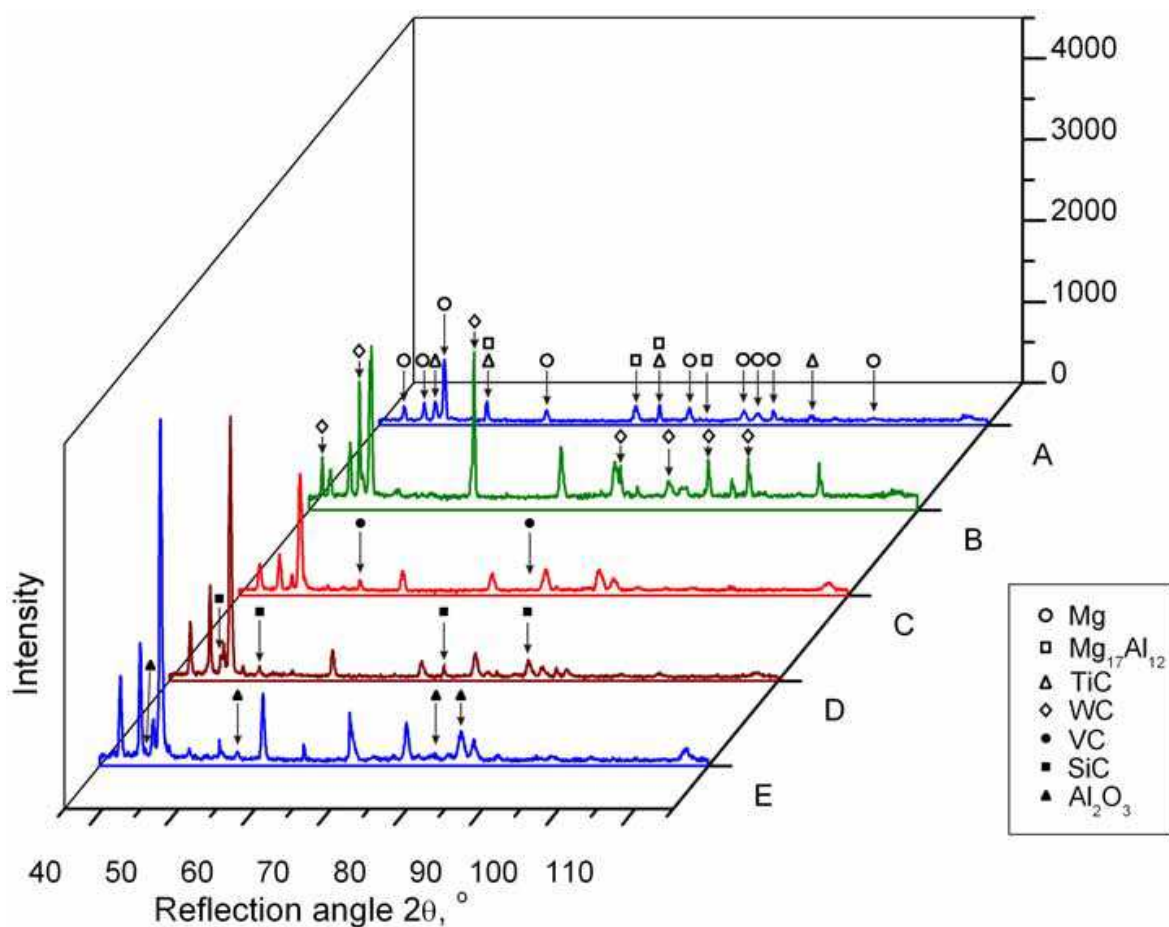
Fig. 28. X ray diffraction pattern of the magnesium cast alloy MCMgAl12Zn1 alloyed with: A – TiC; B – WC; C – VC; D – SiC; E – Al_2O_3

(a)

(b)

(c)
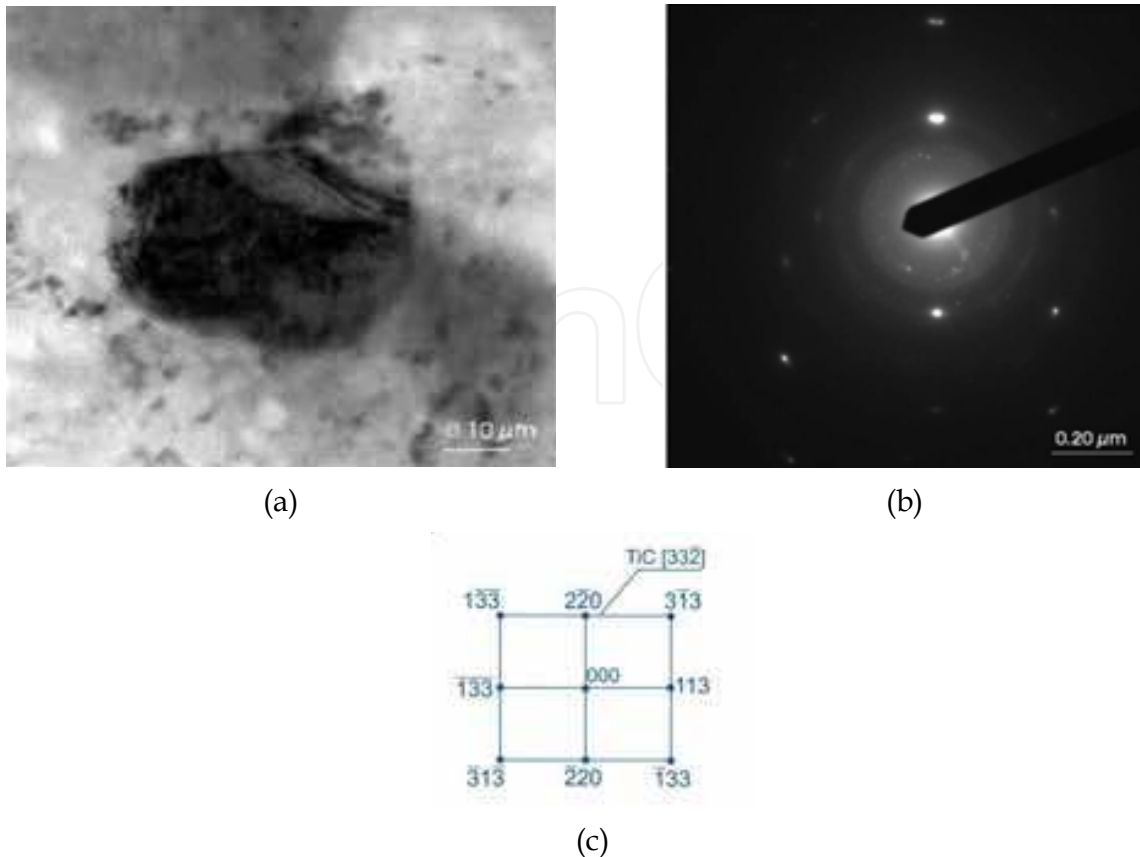
Fig. 29. TEM image of the surface layer of MCMgAl9Zn1 alloy after alloing with TiC:
a) bright field; b) diffraction pattern of area shown in a), c) part of solution for diffraction
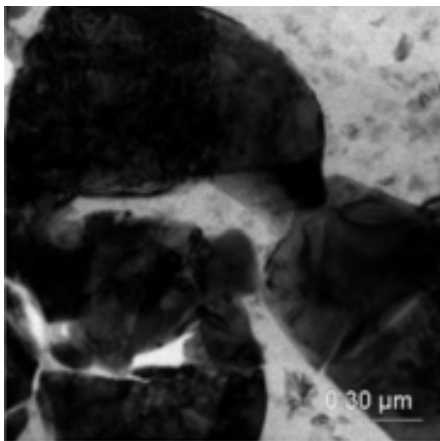pattern shown in b

7. Conclusion

The results are summarized as follows:
- The new developed experimental as-cast cast magnesium alloys MCMgAl12Zn1, MCMgAl9Zn1, MCMgAl6Zn1, MCMgAl3Zn1 are showing an α solid solution microstructure, which is the matrix, intermetallic γ – $Mg_{17}Al_{12}$ phase in a shape of plates, placed manly at grain border regions, needle shaped eutectic (α+γ) as well Mg and Si containing precipitations characterized by edged outlines, also steroidal or needle shaped phases with high Mn and Al concentration are present.
- Solution treatment wit cooling in water and in air causes solution of the γ – $Mg_{17}Al_{12}$ in the matrix and exists only in a small amount together with single phases containing silicon and manganese. Ageing with air cooling after solution treatment in water causes a precipitation of homogeny distributed $Mg_{17}Al_{12}$ in the matrix in form of needle shaped precipitations, coming into existence also in form of pseudo-eutectic areas. Dispersive precipitations in the solid solution in the aged magnesium alloys have in mostly investigated an preferred crystallographic orientation with the matrix. A part of the show a relation like:

$$(1\bar{1}01)\alpha\text{-Mg}\|(10\bar{1})Mg_{17}Al_{12}$$
$$[11\bar{2}0]\alpha\text{-Mg}\|[111]Mg_{17}Al_{12}$$

γ - $Mg_{17}Al_{12}$ phase precipitation have mostly a shape of rods and plates, a prevailing growing direction are the directions from the <110> family of the α-Mg phase.

- Precipitation hardening causes changes of mechanical properties. The highest hardness increase in as cast alloy and after ageing show casts from the MCMgAl12Zn1 alloy with a value of 75.4 and 94.6 HRF. The smallest average mass loss of the tribologic examined samples, connected with an increased hardened phase amount, particularly the $Mg_{17}Al_{12}$ phase and the applied heat treatment, occurs for the MCMgAl12Zn1 alloys.

- The highest strength value in as-cast state have the MCMgAl6Zn1 and MCMgAl3Zn1 alloys, which have also the highest elongation in as-cast state. It was showed , that an increase of the Al concentration from 6 to 12% decreases the strength value in as-cast state. The maximal yield strength was achieved for the MCMgAl12Zn1 alloys, slightly higher for the MCMgAl9Zn1 alloy. In as-cast state the lowest elongation show the MCMgAl12Zn1 material with 12% aluminium content, more then fife times lower compared to the elongation value of the MCMgAl3Zn1 alloy. After ageing with cooling in air the maximum strength increase of 124 1.7 MPa and a yield strength of 20 MPa was achieved for the MCMgAl12Zn1 alloy. The alloys after ageing are characterized by a slightly decreasing elongation value compared to the as-cast state.
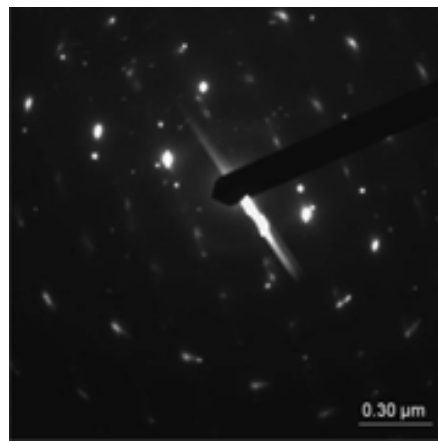
(a)   (b)
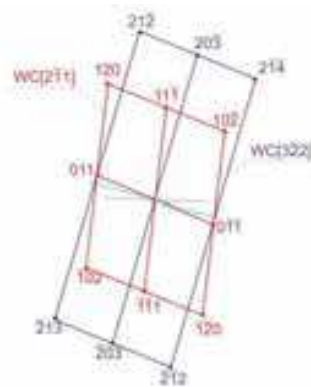
(c)

Fig. 30. TEM image of the surface layer of MCMgAl9Zn1 alloy after alloing with WC:
a) bright field; b) diffraction pattern of area shown in a), c) part of solution for diffraction pattern shown in b
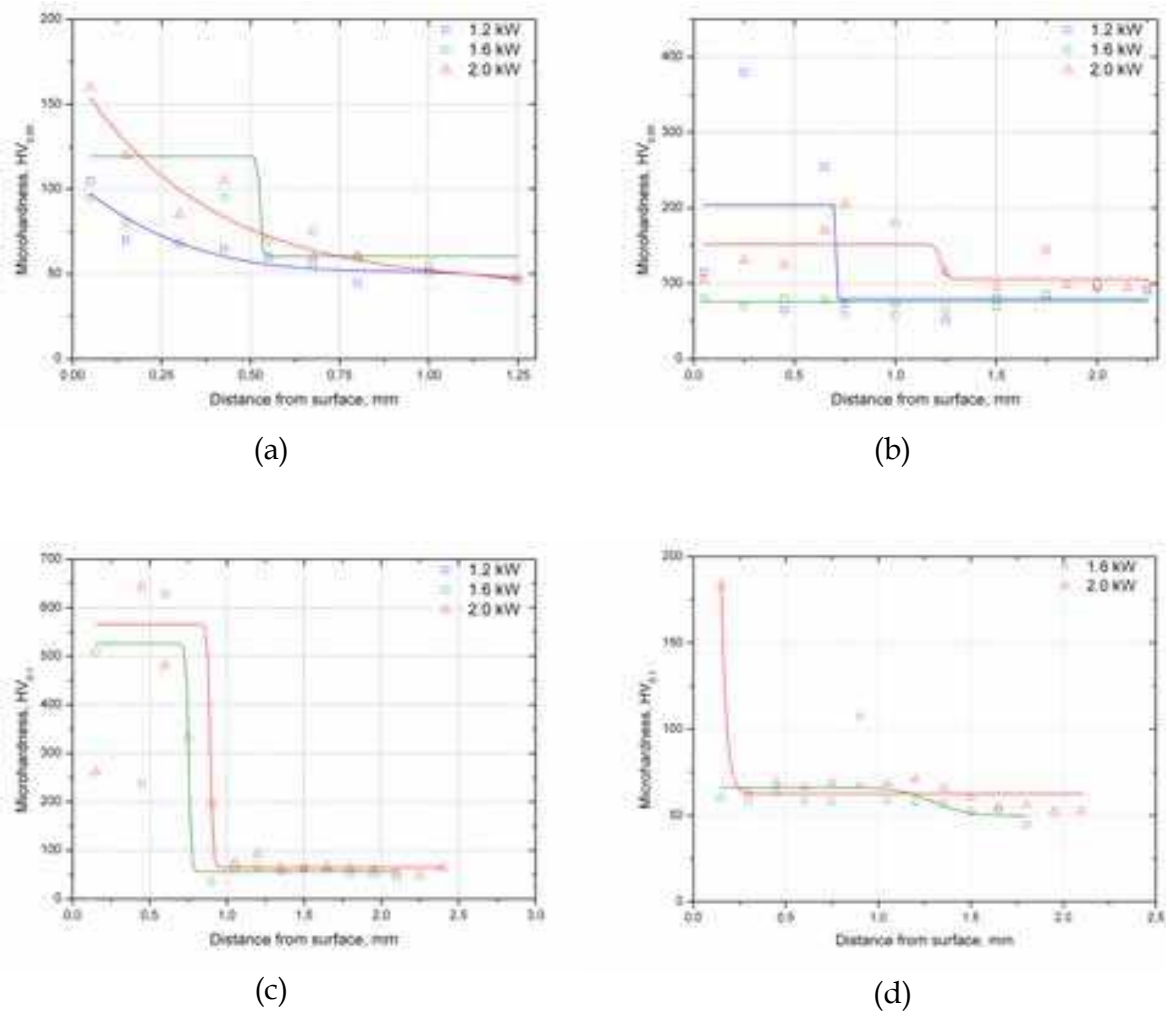
(a)

(b)

(c)

(d)

Fig. 31. Micro hardness change of the surface layer of the magnesium cast alloy: a) MCMgAl6Zn1 alloyed with WC, alloying speed: 0.75 m/min, b) MCMgAl6Zn1 alloyed with TiC, alloying speed: 0.75 m/min, c) MCMgAl12Zn1 alloying speed SiC, alloing speed: 0.75 m/min, d) MCMgAl9Zn1 alloyed with Al_2O_3, alloying speed: 0.50 m/min

- Derivative thermo-analysis performed allowed to achieve several representative cooling, crystallization and calorimetric curves with characteristics points of crystallisation process for magnesium alloys which were presented in Fig. 17, 18. Description of characteristics points obtained from thermal-derivative analysis was presented in Table 7 and made it possible to get better understanding of the thermal processes occurred during crystallization kinetics of the investigated Mg alloys.
- Solidification parameters are affected by the cooling rate. The formation temperatures of various thermal parameters are shifting with an increasing cooling rate. Increasing the cooling rate increases significantly the Mg nucleate temperature and decreases the solidus temperature simultaneously widens a solidification range.
- As expected, the results show that grain size reduces as the cooling rate increases. Increasing the cooling rate increases hardness and compressive ultimate strength of the examined magnesium alloys.

- Investigations of the surface layers carried out confirm that alloying of the surface layer of the Mg-Al-Zn casting magnesium alloys is feasible using the HPDL high power diode laser ensuring better properties compared to alloys properties after the regular heat treatment after employing the relevant process parameters. The structure of the remelted zone is mainly dendritic of primary magnesium with eutectic of phase α-Mg and intermetallic phase γ-Mg17Al12. Magnesium alloys with aluminum concentration 9 and 12 wt. % reveal heat affected zone in opposition to alloys with aluminum concentration 3 and 6 wt. %.
- Surface layers fabricated by alloying with VC, TiC, WC, SiC and Al_2O_3 the casting magnesium alloys (MCMgAl12Zn1 and MCMgAl9Zn1) demonstrate the clear effect of the alloyed material, parameters of the alloying process, and especially of the laser beam power and type of the ceramic particles on structure and mechanical properties of the surface layers. Due to laser alloying structure develops with the clear refinement of grains containing mostly the dispersive particles of the carbide and oxide used in the casting magnesium alloy matrix.
- Microhardness investigation shows that hardness increases in the alloyed zone to values from 100 to 700 HV0, 1, when hardness of substrate is in the range from 50 to 90 HV0,1. The microhardness value growth is an effect of refinement of a magnesium alloys structure and very hard carbides particles appearance within surface layer area.

8. Acknowledgements

9. References

Bachmann, F. (2003). Industrial applications of high power diode lasers in materials processing, *Applied Surface Science*, Vols. 208-209, 125-136, ISSN: 0169-4332

Backuerud, L.; Chai, G. & Tamminen, J. (1990). *Solidification characteristics of aluminum alloys Vol.2 Foundry Alloys*, AFS Skanaluminium, ISBN: 0874331196, Sweden

Baker, H. (1999). *ASM Specialty Handbook. Magnesium and Magnesium Alloys*, Avedesian (Ed.), ASM International, ISBN: 0871706571, USA

Barnes, S.; Timms, N. & Bryden, B. (2003). High power diode laser cladding, *Journal of Material Processing Technology*, Vol. 138, 411-416, ISSN: 0924-0136

Cao, X.; Jahazia, M.; Fournierb, J. & Alainb. M. (2008). Optimization of bead spacing during laser cladding of ZE41A-T5 magnesium alloy castings, *Journal of Materials Processing Technology*, Vol. 205, 322-331. ISSN: 0924-0136

Dobrzański, L.A. & Tański, T. (2009). Influence of aluminium content on behaviour of magnesium cast alloys in bentonite sand mould, *Solid State Phenomena*, Vols. 147-149, 764-769, ISSN: 1012-0394

Dobrzański, L.A.; Tański, T.; Domagała, J.; Król, M.; Malara, S. & Klimpel, A. (2008). Structure and properties of the Mg alloys in as-cast state and after heat and laser

treatment, *Journal of Achievements in Materials and Manufacturing Engineering*, Vol. 31, 123-147, ISSN: 1734-8412

Dutta Majumdar J.; Galun, R.; Mordike, B.L. & Manna, I. (2003). Effect of laser surface melting on corrosion and wear resistance of a commercial magnesium alloy, *Materials Science and Engineering: A*, Vol. 361, 119-129, ISSN: 0921-5093

Emadi, D.; Whiting, L.V.; Nafisi, S. & Ghomashchi, R. (2005). Applications of thermal analysis in quality control of solidification processes, *Journal of Thermal Analysis and Calorimetry*, Vol. 81, 235-242, ISSN: 1572-8943

MacKay, R.; Djurdjevic, M. & Sokolowski, J.H. (2000). The effect of cooling rate on the fraction solid of the metallurgical reaction in the 319 alloy, *AFS Transaction*, Vol. 108, 521-530

Fajkiel, A. & Dudek, P. (2004). High performance advanced castings. Pt 2, Examples of application of castings from non-ferrous metals alloys, *Odlewnictwo – Nauka i Praktyka*, Vol. 1, 18-22, ISSN: 1730-2250

Guldberg, S. & Ryum, N. (2000). Microstructure and crystallographic orientation relationship in directionally solidified Mg–Mg$_{17}$Al$_{12}$-eutectic, *Materials Science and Engineering A*, Vol. 289, 143-150, ISSN: 0921-5093

Horst, E.F. & Mordike, B.L. (2006). *Magnesium Technology. Metallurgy, Design Data, Application*, Springer-Verlag, ISBN: 978-3-540-20599-9, Berlin Heidelberg

Kainem, K.U. (2003). *Magnesium – Alloys and Technology*, Wiley-VCH Verlag GmbH & Co., ISBN: 3-527-30570-X, Weinheim, Germany

Kasprzak, W.; Sokolowski, J.H.; Sahoo, W. & Dobrzanski, L.A. (2008). Thermal and structural characteristics of the AZ50 magnesium alloy, *Journal of Achievements in Materials and Manufacturing Engineering*, Vol. 29, 179-182, ISSN: 1734-8412

Kiełbus A., Rzychoń, T. & Cibis, R. (2006). Microstructure of AM50 die casting magnesium alloy, *Journal of Achievements in Materials and Manufacturing Engineering*, Vol. 18, 135-138, ISSN: 1734-8412

Kierkus, W.T. & Sokolowski, J.H. (1999). Recent Advances in CCA:A new method of determining baseline equation, *AFS Transactions*, Vol. 66, 161-167

Maltaisa, A.; Dubé, D.; Fiseta, M.; Larochea, G. & Turgeon, S. (2004). Improvements in the metallography of as-cast AZ91 alloy, *Materials Characterization*, Vol. 52, 103-119, ISSN: 1044-5803

Rzychoń, T. & Kiełbus, A. (2007). Microstructure of WE43 casting magnesium alloys, *Journal of Achievements, in Materials and Manufacturing Engineering*, Vol. 21, 31-34, ISSN: 1734-8412

Tański, T.; Dobrzański, L.A. & Čížek, L. (2007). Influence of heat treatment on structure and properties of the cast magnesium alloys, *Journal of Advanced Materials Research*, Vol. 15-17, 491-496, ISSN: 1022-6680

Vollertsen, F.; Partes, K. & Meijer, J. (2005). State of the art of laser hardening and cladding, *Proceedings of the Third International WLT-Conference on Lasers in Manufacturing 2005*, Munich, June 2005, Munich

Yadroitsev, I.; Bertrand, P.; Laget, B. & Smurov, I. (2007). Application of laser assisted technologies for fabrication of functionally graded coatings and objects for the

International Thermonuclear Experimental Reactor components, *Journal of Nuclear Materials*, Vol. 362, Nos. 2-3, 189-196, ISSN: 0022-3115

"Method and Apparatus for Universal Metallurgical Simulation and Analysis" – *United States Patent, Patent No.: US 7,354,491 B2*, Date of Patent: Apr. 8 (2008).
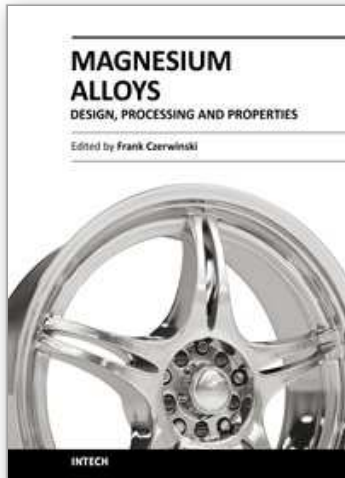
Magnesium Alloys - Design, Processing and Properties
Edited by Frank Czerwinski

ISBN 978-953-307-520-4

Hard cover, 526 pages

Publisher InTech

Published online 14, January, 2011

Published in print edition January, 2011

Scientists and engineers for decades searched to utilize magnesium, known of its low density, for light-weighting in many industrial sectors. This book provides a broad review of recent global developments in theory and practice of modern magnesium alloys. It covers fundamental aspects of alloy strengthening, recrystallization, details of microstructure and a unique role of grain refinement. The theory is linked with elements of alloy design and specific properties, including fatigue and creep resistance. Also technologies of alloy formation and processing, such as sheet rolling, semi-solid forming, welding and joining are considered. An opportunity of creation the metal matrix composite based on magnesium matrix is described along with carbon nanotubes as an effective reinforcement. A mixture of science and technology makes this book very useful for professionals from academia and industry.

INTECH
open science | open minds